POLITECNICO
MILANO 1863

SCUOLA DI INGEGNERIA INDUSTRIALE
E DELL'INFORMAZIONE

Design and implementation of a laser measurement system for loudspeaker vibrational behaviour characterization

Tesi di Laurea Magistrale in
Music and Acoustic Engineering

Author: **Lorenzo Lellini**

Student ID: 974765
Advisor: Prof. Giuseppe Bertuccio
Co-advisor: Dott. Marco Zanettini
Academic Year: 2022-2023

Abstract

Loudspeaker design poses numerous challenges, necessitating careful consideration of various factors to achieve the desired performance. The designer must address parameters such as material selection, evaluation of mechanical limitations, and production costs. Gaining an understanding of the vibrational behaviour of a loudspeaker cone can greatly assist in making informed design choices. Indeed, the behaviour of the vibrating membrane of a loudspeaker, which significantly impacts its radiation characteristics, is intricately linked to the behaviour of its constituent components. An analytical tool capable of assessing the entire vibrating surface of a loudspeaker, utilizing measurements obtained through a Laser Doppler Vibrometer, can provide valuable information such as the total sound pressure level (SPL), accumulated acceleration level (AAL), or the breakdown of vibrational behaviour into distinct contributions. The objective of this study is to develop and implement a tool capable of conducting such analyses. Following an examination of the theoretical aspects necessary for achieving the desired outcomes, the tools, methods, and constraints involved in their attainment will be thoroughly analyzed. Lastly, results validating the measurement tool will be presented and compared.

Keywords: Electroacoustics, Loudspeakers, Vibration Analysis, Laser Measurements, Signal Processing, MATLAB

Abstract in lingua italiana

La progettazione di altoparlanti presenta molte sfide e, al fine di ottenere un risultato con il comportamento desiderato, è necessario considerare molti aspetti. L'analisi e la scelta dei materiali, la valutazione dei vincoli meccanici e dei costi di produzione sono solo alcuni dei parametri con cui il progettista deve confrontarsi. Comprendere il comportamento vibrazionale del cono di un altoparlante può sicuramente aiutare nelle scelte di progettazione. Infatti, il comportamento della membrana vibrante di un altoparlante, che influenza anche in modo significativo il suo comportamento di radiazione, è direttamente legato al comportamento dei singoli componenti di cui è composto. Uno strumento che può analizzare l'intera superficie vibrante di un altoparlante tramite diverse misurazioni effettuate con un vibrometro laser e ottenere informazioni come il livello di pressione sonora (SPL), il livello di accelerazione accumulata (AAL) o la suddivisione del comportamento vibrazionale in diversi contributi si dimostra certamente utile per i progettisti di altoparlanti. Lo scopo di questo lavoro è progettare e implementare uno strumento in grado di effettuare questo tipo di analisi. Dopo uno studio degli aspetti teorici necessari per ottenere i risultati desiderati, saranno analizzati gli strumenti, i metodi e i vincoli per ottenerli. Infine, saranno presentati e confrontati i risultati volti a convalidare lo strumento di misura.

Parole chiave: Elettroacustica, Altoparlanti, Analisi delle Vibrazioni, Misurazioni con Laser, Elaborazione dei Segnali, MATLAB

Contents

Introduction

Loudspeaker design is a complex process that requires careful consideration of various factors to achieve optimal performance. Designers face challenges in selecting appropriate materials, evaluating mechanical limitations, and managing production costs. Understanding the vibrational behaviour of a loudspeaker cone plays a crucial role in making informed design choices, as it significantly influences the loudspeaker's radiation characteristics. Analyzing the behaviour of the vibrating membrane and its constituent components can provide valuable insights into the overall performance of the loudspeaker.

To assess the entire vibrating surface of a loudspeaker, a robust analytical instrument is needed. This instrument should utilize measurements obtained through a Laser Doppler Vibrometer (LDV), a precise instrument capable of capturing detailed vibration data. By employing this instrument, valuable information such as the total sound pressure level (SPL), accumulated acceleration level (AAL), and the breakdown of vibrational behaviour into distinct in-phase, anti-phase and quadrature contributions can be obtained. Such information can aid designers in understanding the performance limitations and potential areas for improvement in loudspeaker design.

The objective of this work is to develop and implement a instrument capable of conducting comprehensive analyses of loudspeaker vibrations. Initially, the theoretical aspects essential for achieving the desired outcomes will be examined. Subsequently, tools, methods, and constraints involved in the development and implementation of this analytical instrument will be thoroughly analyzed. Finally, the study will present and compare results validating the effectiveness and accuracy of the measurement instrument.

By addressing these objectives, this research aims to contribute to the field of loudspeaker design by providing a comprehensive and reliable instrument for analyzing the vibrational behaviour of loudspeaker membranes. This instrument has the potential to enhance the understanding of loudspeaker performance and guide designers in making informed decisions, leading to improved loudspeaker designs with enhanced sound quality and efficiency.

1 | Root causes of a nonlinear behaviour in professional loudspeakers

1.1. Loudspeaker history

The evolution of loudspeakers can be traced back to the late 19th century. The inventor Alexander Graham Bell is credited with the invention of the first practical telephone in 1876, which included a device called a "*loud-speaking telephone*" that allowed people to speak to each other at a certain distance in normal voice, rather than having to shout. It consisted of a diaphragm made of a thin sheet of metal or paper that was attached to a magnet and suspended in a coil of wire. When an electrical current passed through the coil, it would produce a magnetic field that caused the diaphragm to vibrate, producing sound waves.

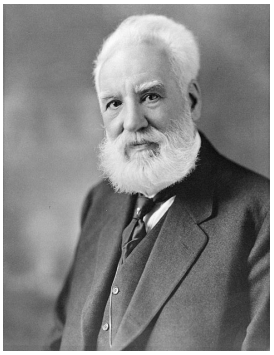

Figure 1.1: Alexander Graham Bell, the loudspeaker inventor.

Another important contribution to the modern loudspeaker development is the research paper of Chester W. Rice and Edward W. Kellogg at General Electric in 1925 that was important in establishing the basic principle of the direct radiator loudspeaker with a small coil-driven mass-controlled diaphragm in a baffle with a broad midfrequency range of uniform response.

The application of the technology at this time was primarily limited to telephony and public address systems. It was not until the early 20th century that the use of loudspeakers began to see wider applications, particularly in the field of radio communications. The incorporation of loudspeakers into radio sets during the 1920s contributed significantly to the spreading of the technology, thereby increasing its scope of usage.

The 1930s saw the development of magnetic drivers that significantly improving sound quality, resulting in more compact and efficient loudspeakers. These developments saw the widespread use of loudspeakers in various audio equipment such as record players and Hi-Fi stereos during the mid-20th century. The increasing demand for high-quality audio equipment asked for innovative materials and designs in loudspeaker technology, which resulted in more accurate and powerful sound reproduction during the 1970s and 80s.

The popularity of loudspeakers continued to grow, with advancements in technology resulting in the incorporation of cutting-edge innovations such as wireless connectivity and voice recognition. Today, loudspeakers have become ubiquitous in everyday life, found in everything from smartphones to concert venues. The advent of digital signal processing and artificial intelligence has further revolutionized loudspeaker technology, resulting in more sophisticated and advanced products with unparalleled sound quality.

Currently, professional loudspeakers find widespread usage in various fields, ranging from live music performances, cinema, and home entertainment to public address systems and educational settings. In live music events, large-scale loudspeaker systems are deployed to provide high-quality sound reinforcement for the audience, enabling performers to deliver their performances with precision and clarity. Similarly, in cinema, powerful loudspeakers are used to reproduce the film's soundtrack with a high degree of accuracy, immersing the audience in the movie's world.

In educational field, loudspeakers are used in lecture halls and classrooms to amplify the voice of the lecturer, ensuring that students can hear and understand the content of the lecture. Public address systems in stadiums and other large venues employ loudspeakers to provide information and announcements to a large audience, ensuring everyone can hear and stay informed.

The use of professional loudspeakers has also become increasingly prevalent in the field of home entertainment, with many people now seeking to recreate the cinema experience in the comfort of their own homes [1]. High-end home theater systems often feature powerful loudspeakers that provide exceptional sound quality, immersing viewers in a rich and dynamic audio experience.

When attending a modern live concert or event, the immersive experience is shaped by various factors, but one element that stands out is the quality of the sound. Professional loudspeakers play a pivotal role in delivering exceptional audio to large audiences, ensuring that every note, beat, and lyric reaches the listener with precision and impact.

Concerts and events are very demanding environments for loudspeakers. They are subjected to constant transportation, rigorous setups and tear-downs and exposure to varying weather conditions. Therefore, in the last two decades durability and quality becomes a paramount consideration for professional loudspeakers to withstand the rigors of touring and event production.

1.2. Loudspeaker anatomy and fundamental parameters

An electrodynamic or moving-coil loudspeaker is an electromagnetic transducer for converting electrical signals into sounds [2]. Beyond the considerations that can be made on the dimensions of the diaphragm and on the construction techniques, we can classify two main categories of loudspeakers, depending on whether they are dedicated to the reproduction of low or high frequencies. The most general loudspeaker model is represented in figure 1.2. Each single component contributes to the overall response of the loudspeaker and the choice of different materials and shapes greatly influences the final result. In general, loudspeaker is a highly nonlinear system and its components characteristics strongly influence its nonlinear behaviour [3].

The *diaphragm* or *cone* is a cone made from a suitably light and stiff material (usually treated paper for low frequency loudspeakers and titanium, aluminium or beryllium for high frequencies loudspeakers [4]), although most of the stiffness comes from the fact that it is conical. In the center of the diaphragm there is a *dust cap*, which guards against metallic dust fouling the magnetic gap and prevents sound from the back of the diaphragm leaking through to the outside world.

Attached to the apex of the cone there is a coil former on which the *coil* is wound. This coil is located in the gap of a magnetic path, comprising a *pole piece* and *pole plate*, where the magnetic flux is produced by a *permanent magnet*, which is held in place by a *basket* structure. The diaphragm is supported at the perimeter and near the voice coil respectively by *surround* and *spider*[1], preventing it from moving in the radial direction.

[1]The name "spider" originates from the early electrodynamic loudspeakers in which the cone was supported by a spider-like slotted disk that was anchored to the pole piece in place of the dust cap.

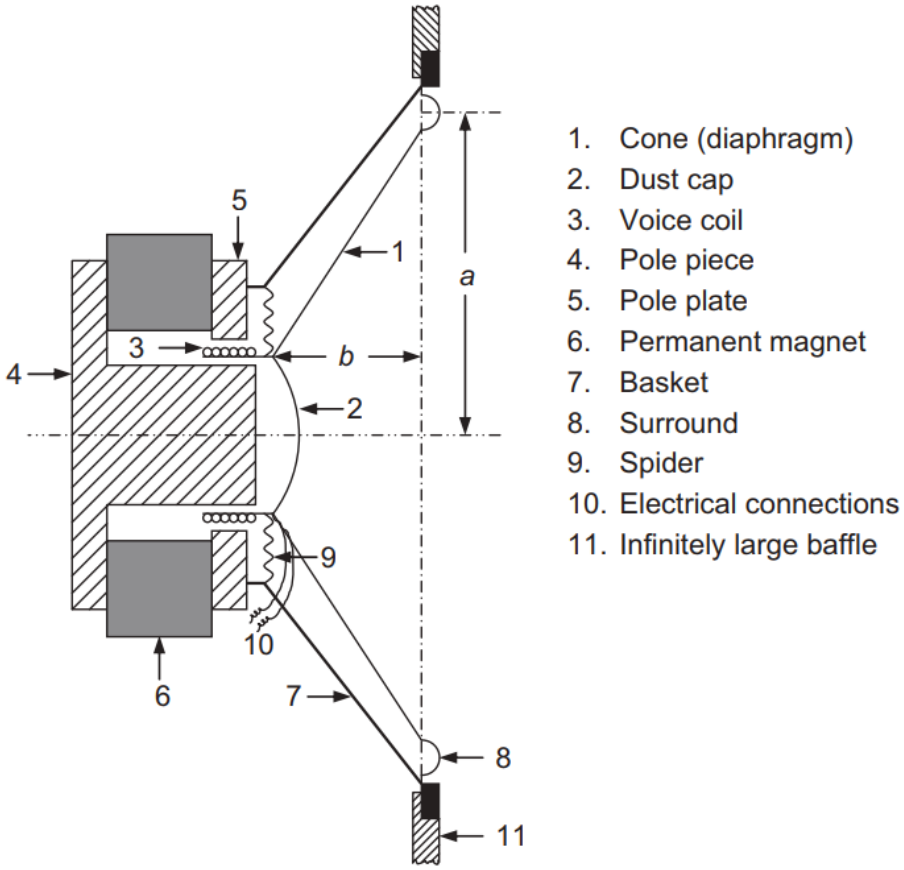

Figure 1.2: Cross-sectional sketch of a direct-radiator loudspeaker assumed to be mounted in an infinite baffle [2].

When an audio signal is applied to the *electrical connections*, the resulting current interacts with the magnetic field in the air-gap produced by the permanent magnet creating a magneto-motive force which causes a translatory movement of the voice coil and, hence, of the cone to which it is attached. The movement of the cone displaces the air molecules at its surface thus producing sound waves.

At high frequencies, however, vibrations from the center travel outward towards the edge of the cone in the form of waves. The results of these traveling waves and of resonances in the cone itself are to produce irregularities in the frequency response curve at the higher frequencies and to influence the relative amounts of sound radiated in different directions [2], as shown in chapter 2. Loudspeaker can be modeled as the interaction between three domains: electrical, mechanical and acoustical. It can be defined as a mass-spring-damper system from the mechanical point of view [5] and, exploiting the analogies between electrical, mechanical and acoustical elements [2], can be obtained a circuit representation of it that takes into account the three domains.

In order to characterize the equivalent loudspeaker circuit, we must define several elements involved. The physical parameters of a loudspeaker can be easily translated into the corresponding Thiele-Small parameters. The Thiele-Small parameters are known as the valuable specifications that determine the low-frequency performance of loudspeakers. The parameters are named after two Australian loudspeaker engineers: Richard H. Small and A. Neville Thiele. All parameters are related to equivalent circuit components as capacitors, inductors, and resistors. We can divide the Thiele-Small parameters in three different sets [6–14]:

The **Electromechanical parameters**:

- Effective diaphragm area S_D
- Moving mass M_{MS}
- Suspensions mechanical stiffness K_{MS}, mechanical compliance $C_{MS} = 1/K_{MS}$ and mechanical resistance $R_{MS} = 1/G_{MS}$, where G_{MS} is the mechanical conductance
- Voice coil inductance L_E and resistance R_E
- Force factor Bl where B is the stationary air-gap magnetic field or flux density in Tesla and l is length of wire in meters on the voice-coil winding

The **Small-Signal parameters**:

- Resonance Frequency f_s
- Acoustic compliance of driver, expressed as an equivalent volume of air V_{AS}
- Electrical quality factor (or electrical damping) Q_{es}
- Mechanical quality factor (or mechanical damping) Q_{ms}
- Combined quality factor (or total damping) Q_{ts}

The **Large-Signal parameters**:

- Maximum cone excursion X_{max}
- Displacement-limited electrical input power rating in watt P_{ER}
- Volume displacement $V_D = S_D \cdot X_{max}$

Considering these parameters we can easily retrieve the equivalent loudspeaker *electro-mechano-acoustical* analogous circuit model shown in figure 1.3 where the mechanical radiation admittance Y_{AR} and the generator resistance Rg have been included.

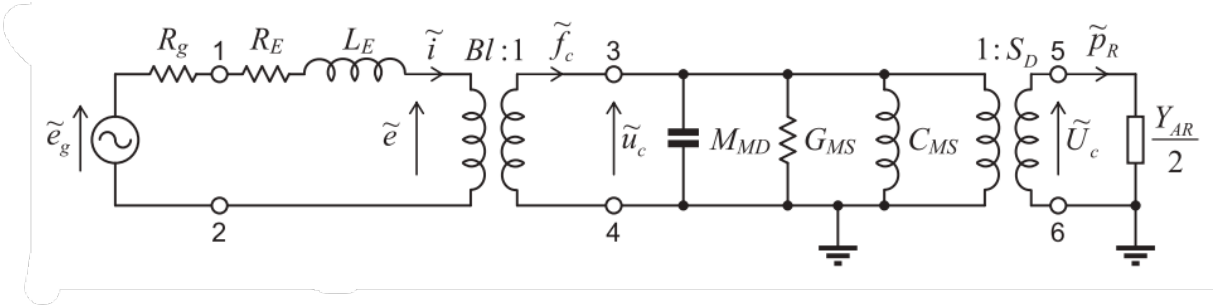

Figure 1.3: Electro-mechano-acoustical analogous circuit of the admittance type [2].

Since the purpose of this work is not to analyze the loudspeaker from a circuital point of view but to characterize it from a vibrational point of view by designing a reliable measuring instrument that can provide useful information during the design phase, we will not dwell beyond the electrical aspect but we will focus on the vibrational aspect.

The important concept to understand is that in any case the vibrational behaviour, the frequency response and these fundamental parameters necessary to describe the circuit model of the loudspeaker are closely linked to each other and contribute to the overall response [15–20].

1.3. Loudspeaker membrane vibrational behaviour

At first glance, we can approximate a loudspeaker membrane to a clamped edge circular plate by neglecting the dimension of the z-axis. To understand the behaviour of waves in circular plates, it is essential to grasp the underlying principles. Circular plates, when struck or excited, exhibit a variety of wave patterns, known as modes or resonant frequencies. These modes arise due to the boundary conditions imposed by the circular shape and by the clamping.

Each resonant frequency in a circular plate corresponds to a specific mode, representing the distribution of vibrations across the surface. The simplest and most common mode is the fundamental mode, which has a single nodal line encircling the center of the plate. As the frequency increases, additional nodal lines emerge, forming more complex patterns. These nodal lines are stationary points, areas of no vibration, separating regions of maximal displacement called antinodes. Higher modes exhibit complex nodal patterns, producing beautiful and complex shapes. The boundary conditions imposed by the circular shape significantly affect the behaviour of waves in circular plates. The nodal patterns observed in circular plates are a result of these boundary conditions.

The outer edge of the plate acts as a fixed boundary, restricting the motion of the waves and creating stationary points. Due to the radial symmetry of circular plates, the waves can propagate in all directions. As a result, the nodal patterns exhibit rotational symmetry, with a nodal line encircling the center. This characteristic distinguishes the behaviour of waves in circular plates from those in other geometrical shapes.

Resonance plays a crucial role in the behaviour of waves in circular plates.When a plate is excited at its resonance frequency, it enters a state of harmonic resonance. This resonance occurs when the natural frequency of the plate matches the frequency of the applied stimulus, leading to an amplification of the vibrations. Each mode or resonant frequency of a circular plate corresponds to a specific harmonic. The fundamental mode represents the first harmonic, while higher modes correspond to higher harmonics. The harmonics contribute to the complexity of the nodal patterns, creating visually captivating shapes as the frequency increases.

The equation of motion for a circular plate can be described by the equation 1.1, which relates the plate's deflection to its boundary conditions and applied loads. In polar coordinates (r, θ), the equation is given as:

$$\nabla^4 Z(r,\theta) + k^4 Z(r,\theta) = 0 \tag{1.1}$$

where:

- ∇^4 is the operator $(\partial^4/\partial r^4) + (1/r^2)(\partial^4/\partial\theta^4) + (2/r^3)(\partial^4/\partial r^2\partial\theta^2))$
- k is the wave number
- $Z(r,\theta)$ is the is the deflection of the plate as a function of r and θ

As explained in [21, 22], the solution to the equation of motion in polar coordinates is:

$$Z(r,\theta) = \cos(m\theta + \alpha)[AJ_m(kr) + BI_m(kr)] \tag{1.2}$$

that contains the ordinary Bessel functions $J_m(kr)$ and the hyperbolic Bessel functions $I_m(kr) = j^{-m}J_m(jkr)$. Depending on the boundary conditions, the modal frequencies will change [23, 24] and different patterns of nodal circles and diameters are generated as shown in figure 1.4.

A plus sign in figure 1.4 means a motion towards the viewer while a minus sign is related to a motion away from the viewer [25].

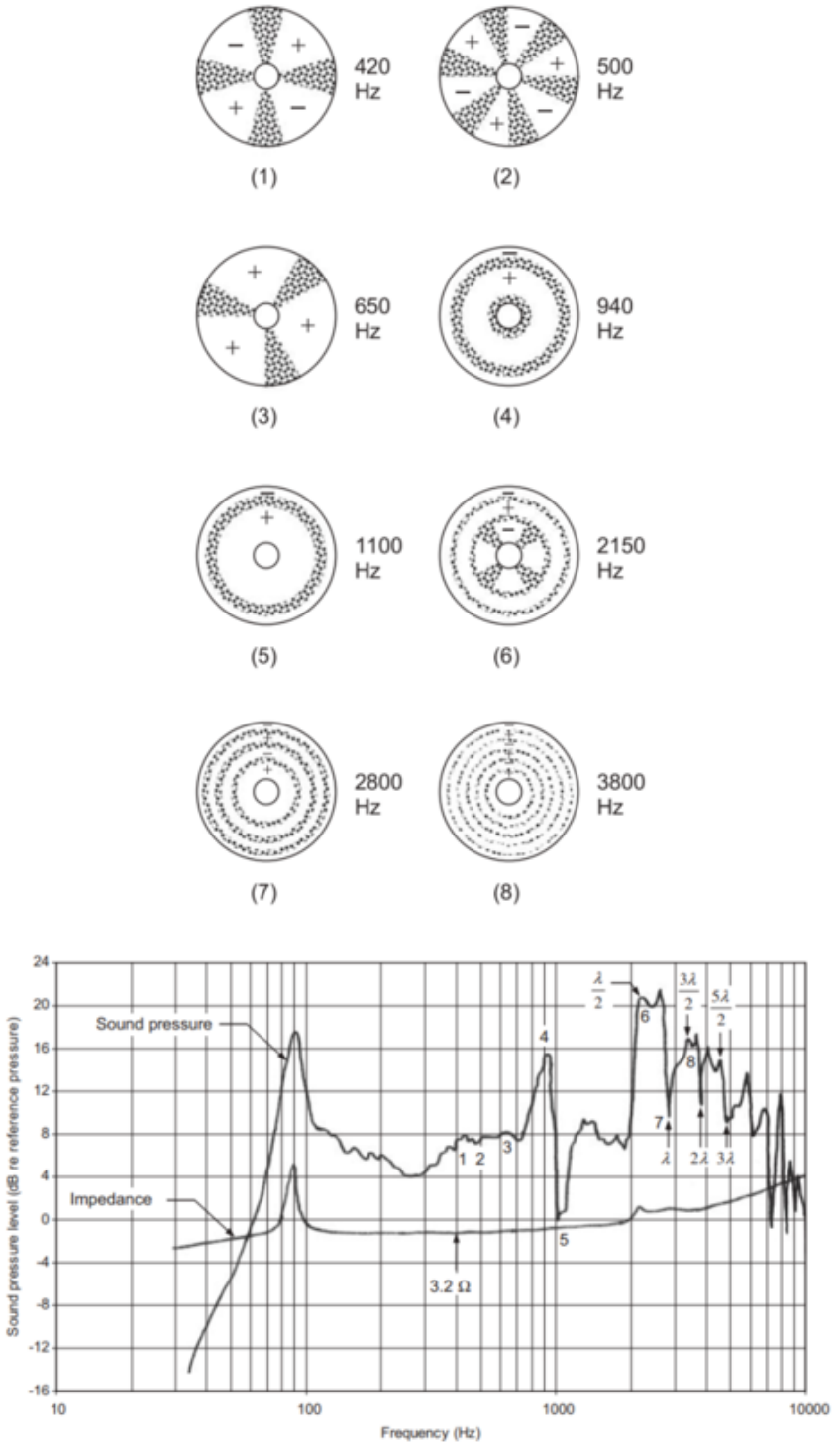

Figure 1.4: Nodal pattern and frequency response of a 200 *mm* loudspeaker cone in a rigid infinite baffle. The shaded and dashed lines indicate lines of small amplitude of vibration. The + and − signs indicate regions moving in opposite directions (opposite phases). In the frequency response plot are indicated the numbers associated with the corresponding nodal line [2, 26].

The mechanical properties of the loudspeaker have a big influence on the frequency response. In fact, the mechanical vibrations depend on the properties of the cone and suspension material, such as mass per area, stiffness, damping, and also on the speaker geometry. At low frequencies the cone is usually sufficiently stiff to move as a whole (**piston mode regime**). But above a certain frequency mechanical bending and longitudinal waves appear on the diaphragm (the so-called cone break-up) creating a complex vibration pattern.

If a certain vibration frequency is observed separately, it is possible to identify more or less distinctive vibration modes which are superposing on each other. Each vibration mode is characterized by a certain mode shape which describes the distribution of certain cone regions vibrating in the same direction (in-phase) or in opposite directions (anti-phase). The total loudspeaker displacement at each frequency can be decomposed on the sum of these components, as shown in section 2.4.

Since the goal of this work is to characterize the membrane, in chapter 2 different measurement grids that will take in account this behaviour will be analyzed.

1.3.1. Radial and circumferential modes

For the mechanical analysis of the cone vibrations a decomposition into radial and circular components can help separating the influence of (certain) vibration modes. An interesting analysis is to separate vibration components according to their relation regarding the radiated sound (chapter 2) [27].

Referring to section 1.3, the measured loudspeaker displacement $x(r, \theta)$, expressed in polar coordinates and depending on radius r and angle θ, can be also expressed as decomposition of radial and circumferential modal components [15]:

$$x(r, \theta) = x_{circ}(r, \theta) + x_{rad}(r) \tag{1.3}$$

The *circular displacement component* is the difference between total vibration and the radial component. The circular component reveals rocking modes [28] and other circumferential modes.

$$x_{circ}(r, \theta) = x(r, \theta) - x_{rad}(r) \tag{1.4}$$

The *radial displacement component* is calculated by averaging the displacement versus the angle θ.

$$x_{rad}(r) = \frac{1}{2\pi} \sum_{\theta=0}^{2\pi} x(r, \theta) \tag{1.5}$$

Circular modes may become dominant in case there is any irregularity at the circumference (such as wires) although the radial component generates the dominant contribution to the on-axis SPL. According to [23, 24], circular components have a negligible effect on the total radiated sound on-axis.
In fact, circular components only contribute significantly to the total SPL off-axis and to the total sound power at higher frequencies [29].

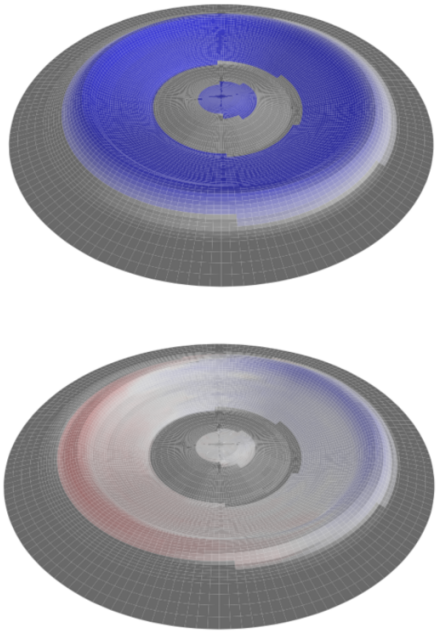

Figure 1.5: Radial (above) and circumferential (below) modes on a loudspeaker membrane example [30].

Theoretically, circular vibrations should hardly occur in loudspeaker cones, because they are not excited by a symmetrically moving voice coil. But in practically small irregularities will also lead to some circular motions in the cone. This component is usually quite small in comparison to the radial motion and might therefore be hardly visible looking only at the total vibration.

On the other hand, circular vibration components can reveal asymmetric vibrations that causes nonlinearity in the response which, while not contributing much to the radiated sound, nevertheless, can introduce distortion due to rubbing of the voice coil in the gap. The reason for these asymmetric vibrations can be a non-symmetric mass distribution of the voice coil or the cone as in the rocking modes presence [15, 31, 32].

1.3.2. Rocking modes

Another undesired aspect of loudspeaker membrane vibrational behaviour are rocking modes that are unwanted tilting movements of the diaphragm. This increases the chance of voice coil rubbing and impulsive distortion (rub and buzz) [33].

Rocking modes main causes are [16]:

- Mass imbalance caused by asymmetrical mass distribution in the moving parts of the transducer.
- Asymmetrical distribution of the suspensions stiffness (the asymmetry generates a moment causing a tilting of the radiator).
- Asymmetrical Force Factor due to the fact that the voice coil is not correctly centered [34, 35].

Rocking modes characterization is therefore fundamental to check for design or manufacturing issues.

1.3.3. Irregular vibrations

Besides radial and circumferential vibrations and rocking modes, there are other irregular vibrations on the diaphragm which usually cannot be neither predicted by finite element analysis. Such irregularities may be caused by unbalanced mass distributions, non uniform density or thickness of the diaphragm caused by intended bracing, and unintended folds generated during shape forming of the cone.

The contributions of irregularities to the total SPL are usually relatively small, but the irregular vibrations may cause excessive nonlinear distortion because the displacement may be much higher at particular points.

Moreover, irregularities in the manufacturing process may cause an uncontrolled vibration of the diaphragm that thus influence the distortion in the response [15, 30, 31].

1.4. Aging and environmental conditions

As loudspeakers age, various components such as cone, voice coil, and suspension may undergo physical changes, leading to a drift in performance. The mechanical properties of these components can deteriorate over time due to fatigue, resulting in reduced sensitivity and mechanical performance, distorted sound reproduction, and compromised frequency response. Moreover, aging can contribute to increased harmonic and intermodulation distortions, further degrading the audio quality.

Environmental conditions, including temperature, humidity, and exposure to dust and pollutants, also exert a significant influence on loudspeaker aging. High temperatures can accelerate the degradation of adhesives and damping materials, leading to decreased structural integrity and compromised performance. Humidity, particularly in humid or coastal areas, can contribute to corrosion and rust formation on metal components, affecting electrical conductivity and overall functionality.

One of the first parts that are affected by aging are the suspensions. The suspension serves the purpose of fixing the voice coil in a well defined resting position during the forced oscillation. The suspension becomes more and more compliant over time changing the loudspeaker properties significantly [36].

Although treatments such as waterproof paints are applied, spiders and surrounds are generally made from materials such as cloth (impregnated with resins) and rubber. The mechanical stress, combined with the environmental conditions, lead to a change in the properties of these materials and to a consequent variation of the parameters seen in the section 1.2 such as the frequency of resonance and the quality factors [37, 38].

2 | Membrane vibrational behaviour characterization

2.1. Measurement goals

From the analysis carried out in the chapter 1, it is evident how the design of a professional loudspeaker can be extremely complex and needs to take many variables into consideration to obtain the best result [20]. A measuring instrument that can characterize the behaviour of the loudspeaker membrane (and therefore its radiation) can certainly help in the design phase. The purpose of this work is therefore to create an easy-to-use measuring instrument that can provide useful information on the membrane vibrational behaviour of a loudspeaker prototype in order to verify the correct design or to highlight design errors or defects in the used materials.

Loudspeaker membrane nonlinear behaviour introduced in chapter 1 can be analyzed by this instrument. Vibrational decomposition described in 1.3.1, 1.3.2 and in 1.3.3 can be easily analyzed and, evaluating the results, the designer can also better understand at what frequencies the loudspeaker is not working properly and which parts of the loudspeaker might be affected.

In addiction to the loudspeakers prototype analysis, another important aspect of this measurement instrument is the possibility to compare the results of the measurements on a real loudspeaker with the ones of a simulation (e.g. in a software as COMSOL). Since the simulation of a loudspeaker is complex and the results obtained are often difficult to compare with experimental measurements [39, 40], in this way, the designer could match the simulation results with the real loudspeaker behaviour, finding the correct physical parameters for the software materials library.

The measurement instrument is developed starting from [41–44] but some more improvements and customization have been implemented. Each part of the instrument is designed to be as versatile and modifiable as possible, allowing for modifications and improvements both at the mechanical and at the software level.

Although similar instrumentation already exists on the market, this work is focused on reproducing this instrument with a higher level of customization (including the possibility of implementing new features not included in the reference commercial instrument) and much lower costs.

2.2. Displacement and acceleration measurement

The goal is to analyze the loudspeaker in a certain frequency range, taking into account the different amplitude response that varies with frequency. The best way to measure membrane displacement in different points without perturbing the system fixing sensors (such as accelerometers) which would affect its membrane is to use a **laser doppler vibrometer (LDV)**, as explained in section 3.1.4. Also important is the stimulus signal used.

In order to properly characterize the vibrational behaviour of the membrane, it is also important to choose the measurement grid in which the position of the various points is defined. As we will see in 2.2.2, it is not trivial to use one grid or another and the results can significantly change. Eventually, it will finally be necessary to derive the acceleration from the displacement laser measurements.

2.2.1. Input signal generation and IR computation

Membrane vibrational behaviour analysis starts from acquiring its displacement. In order to measure it, the exponential sine sweep excitation signal in formula 2.1 (where T is the duration of the sweep) has been used as stimulus to excite the membrane in a certain range of frequencies between f_1 and f_2 [45–47].

$$x(t) = sin\left[\frac{2\pi f_1 T}{ln\left(\frac{2\pi f_1}{2\pi f_2}\right)} \cdot \left(e^{\frac{t}{T}\cdot ln(\frac{2\pi f_2}{2\pi f_1})} - 1\right)\right] \tag{2.1}$$

Since vibration amplitude decreases as frequency increase, a growing 6 dB/oct amplitude shaping was applied to the sine sweep [48].

We are using a +6 dB/oct sine sweep excitation signal $x(t)$ in order to have a constant amplitude in time inverse convolution filter $g(t)$.

In fact, due to the exponential nature of the signal, a constant amplitude in time corresponds to a -3 dB/oct frequency dependence. In order to compensate for vibration amplitude decreasing with increasing frequency, a filter doubling the signal amplitude

for each doubling of time has been applied to the exponential sine sweep, so that a +3 dB/oct behaviour is shown. With this choice, the inverse convolution filter $g(t)$ ends up having constant amplitude with time (that is −3 dB/oct in frequency dependence) and the *Transfer Function Impulse Response* is correctly equalized.

Loudspeaker is a nonlinear system, so a synchronization procedure is needed for proper analysis of higher harmonics. According with [49] and [48], the duration time T of the sine sweep depends on the frequency range and it is computed as:

$$T = k \cdot \frac{\ln(f_2/f_1)}{f_1} \tag{2.2}$$

where $k \in \mathbb{Z}_{\neq 0}$ is an integer number computed by inverting the same equation 2.2 and considering a different time T of the same *non*-synchronized sine sweep, f_1 is the sine sweep start frequency and f_2 is the sine sweep end frequency.

Moreover, an input and output fading of 1200 samples for a sampling frequency of 48000 Hz has been applied to the sine sweep signal.

Applying the formulas 2.1 and 2.2 and considering $f_1 = 10$ Hz and $f_2 = 10000$ Hz, for example, the duration time of a synchronized sine sweep starting from a 2 seconds non-synchronized sine sweep is 2.0723 seconds.

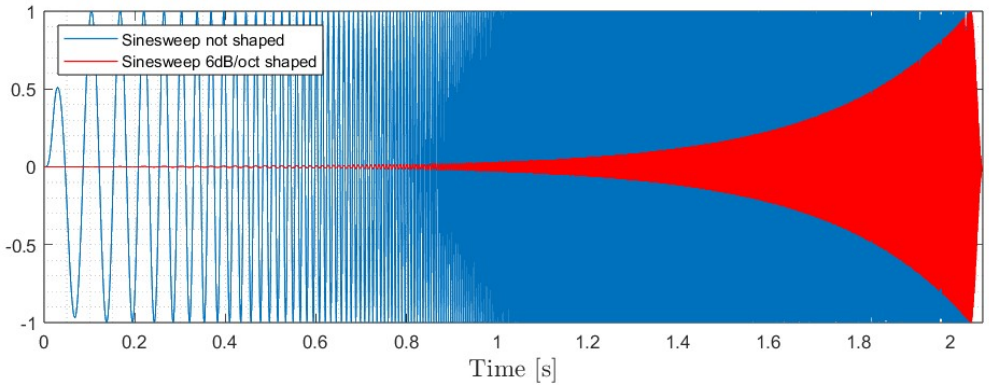

Figure 2.1: Comparison between a constant amplitude and +6 dB/oct amplitude shaped input sine sweep with a frequency range 10Hz - 10kHz.

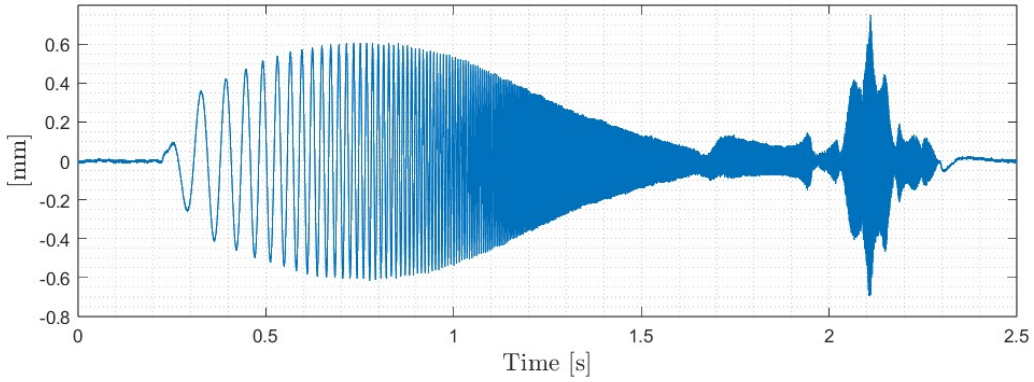

Figure 2.2: Displacement recorded with the laser sensor in a measurement point on the loudspeaker cone surface. In this case, the stimulus frequency range is 10Hz - 10kHz.

Knowing the displacement on a membrane target point $y(t)$ and the sine sweep input stimulus signal $x(t)$, the *Transfer Function Impulse Response* between the measured displacement and the input voltage can be easily calculated by performing a convolution with the constant amplitude inverse sine sweep filter $g(t)$ derived from $x(t)$ [47].

$$h(t) = g(t) * y(t) \tag{2.3}$$

The obtained *Transfer Function Impulse Response* $h(t)$ will be transformed in the frequency domain and used to compute the acceleration, as shown in section 2.2.3.

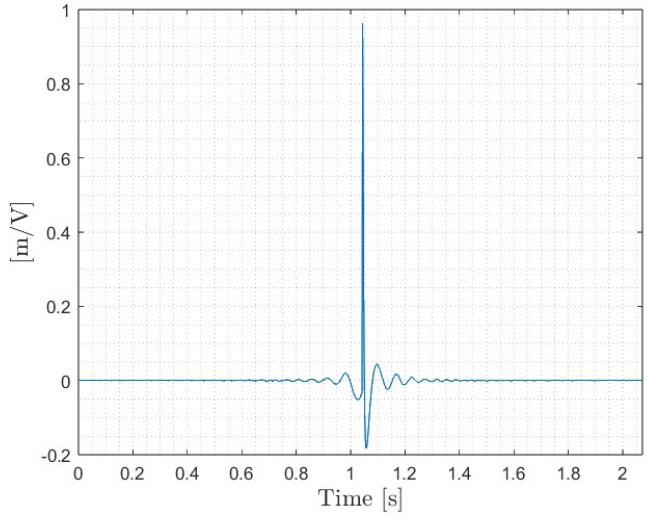

Figure 2.3: Transfer Function IR (Displacement/Input Voltage) for a measured point.

Since for displacement measurements, the laser displacement sensor analog output is connected to a sound card (see section 3.1.1), latency is not constant among different measurements[1].

Since this condition strongly influences the phase of the *Transfer Function*[2] and would the measurement data unusable, a cross-correlation between the IRs has been applied to compensate the latency in post processing step using the `finddelay` MATLAB function. The `finddelay` function uses the `xcorr` function to determine the cross-correlation between each pair of signals at all possible lags specified by the user. The normalized cross-correlation between each pair of signals is then calculated. The estimated delay is given by the negative of the lag for which the normalized cross-correlation has the largest absolute value.

In figure 2.4 a comparison between 20 IRs related to 20 different measurement points on the cone with and without latency compensation is shown.

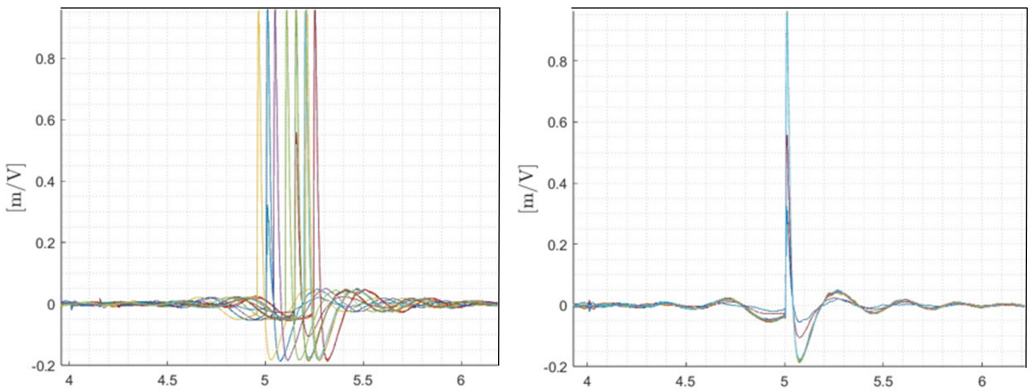

Figure 2.4: 20 IRs related to 20 different measured points without measurement latency compensation (on the left) and with latency compensation (on the right).

2.2.2. Measurement grid

As explained in [48] and [30], in order to properly characterize a loudspeaker diaphragm vibration, hundreds of target points on the cone surface must be measured. Different measurement grid layouts can be chosen in order to have a different resolution in some areas of the diaphragm [41, 42].

[1] Latency can strongly change depending on the used hardware, on the number of active tasks on the computer, on the used OS and on the sound card model.

[2] All the measurement phases are not correctly aligned if the latency is not compensated.

Two types of grid have been designed: a denser one to have a **detailed scan** and a wider one to have an **exploratory scan**. Fixing the stimulus duration according to section 2.2.1, the exploratory measurement duration is about 7 times shorter than the detailed measurement one.

Regardless of the size of the loudspeaker and its effective radiation area S_D [50], the exploratory scan divides the cone in 30 radii (12 degrees between each radius) of 15 measurement points each for a total of 450 measurement points while the detailed scan divides the cone in 80 radii (4.5 degrees between each radius) of 40 measurement points each for a total of 3200 measurement points.

The spacing between the measurement points on the radius depends on the cone size. Moreover, in order to account for the more intricate vibration behaviour in the outer cone region, both for the exploratory and the detailed grid, increasing measurement points density is possible [41, 42].

In this *radial irregular grid spacing*, starting from the center of the cone, the first 2/3 of the points have a certain spacing while the last 1/3 in the outer cone region have half of that spacing.

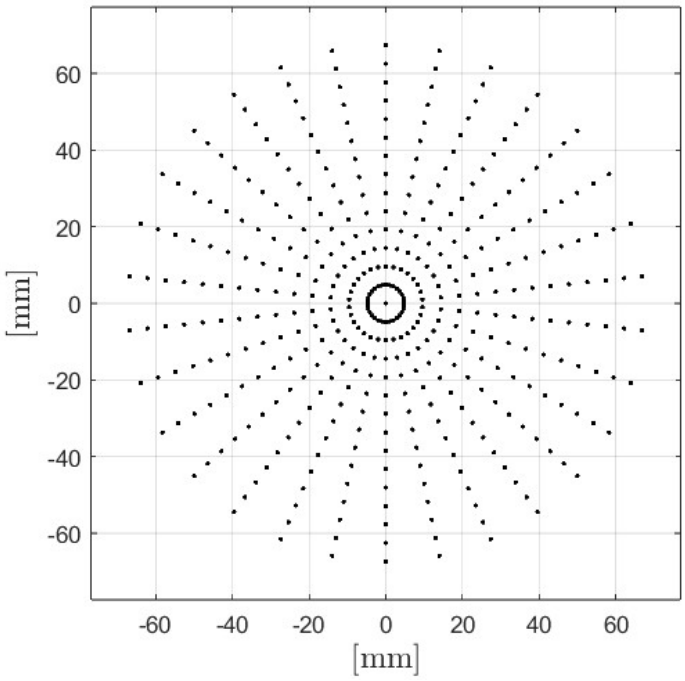

Figure 2.5: Regular spacing exploratory measurement grid for a 6 inches woofer

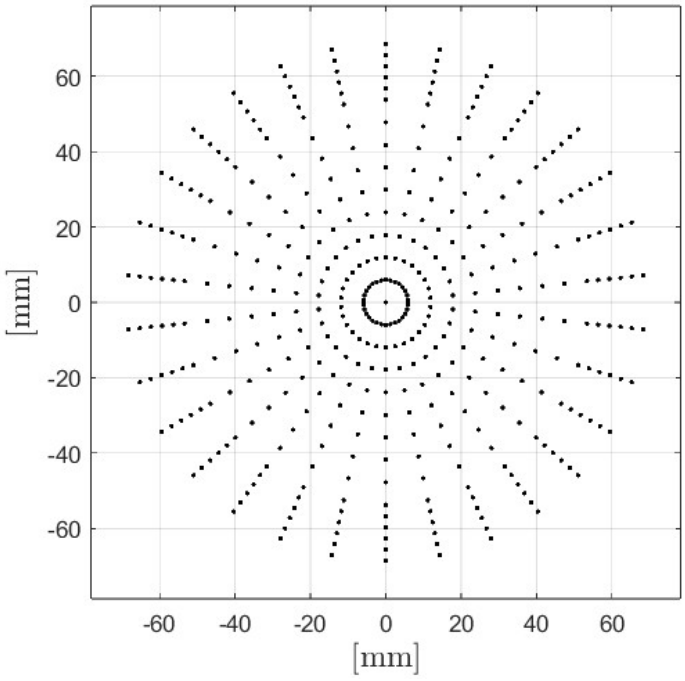

Figure 2.6: Radial irregular exploratory measurement grid for a 6 inches woofer.

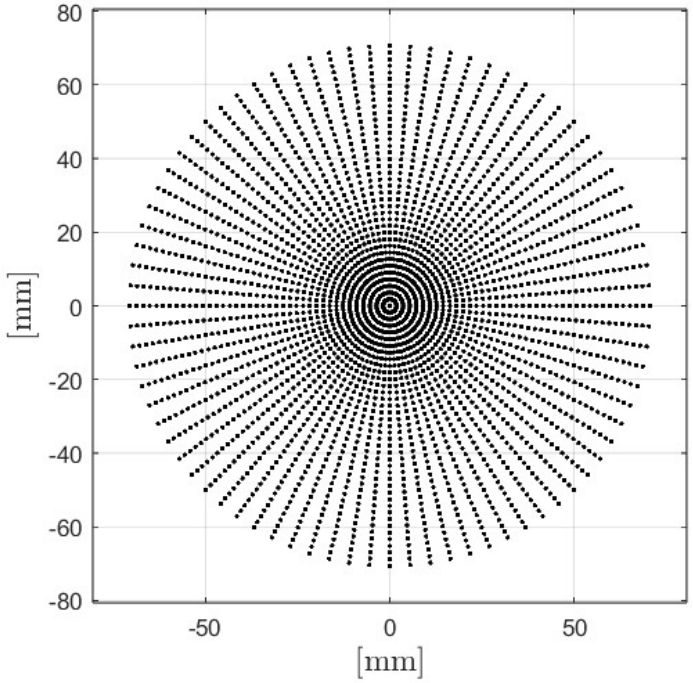

Figure 2.7: Regular spacing detailed measurement grid for a 6 inches woofer.

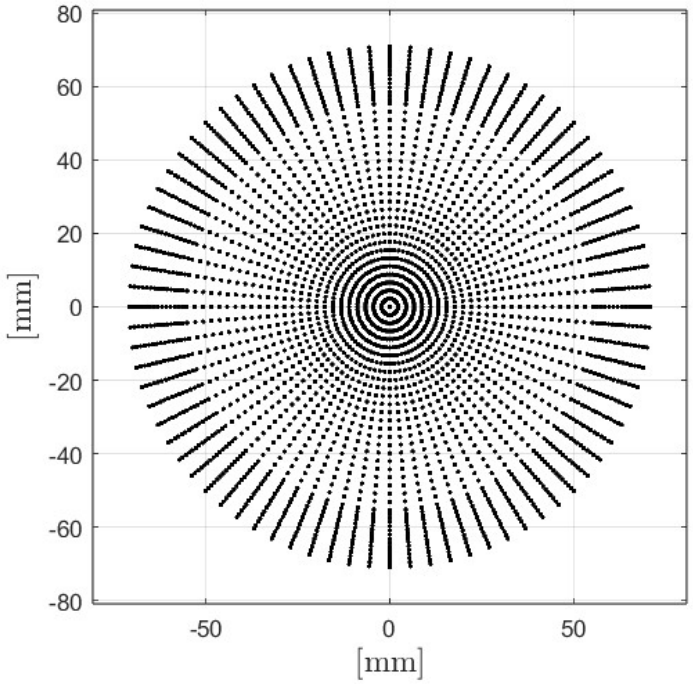

Figure 2.8: Radial irregular detailed measurement grid for a 6 inches woofer.

As we will see in chapter 4, there are several differences in the results by choosing different type of grids. In particular, the choice of the radial irregular spacing one allows to identify with more precision any anti-phase behaviour of the edge. Moreover, the higher measurement point spatial density in the outer region of the cone allows the laser sensor to more accurately measure the irregular profile of that area.

2.2.3. Acceleration computation

For each measurement point, the voltage to displacement *Transfer Function* $X(\omega)$ can be calculated performing a FFT on the *Transfer Function Impulse Response* $h(t)$ 2.3. The voltage to acceleration *Transfer Function* $A(\omega)$ can then calculated from $X(\omega)$ with the following equation:

$$A(\omega) = -\omega^2 \cdot X(\omega) = -(2\pi f)^2 \cdot X(\omega) \tag{2.4}$$

where f is the frequency vector used in the analysis.

2.3. Accumulated Acceleration Level (AAL) and Sound Pressure Level (SPL)

Starting from measured surface displacement, this project aims to predicting the produced sound pressure, in order to assess the importance of modal behaviour on sound emission and to establish a quantitative connection between particular kinds of modes and particular effects in the pressure response.

Approximating the loudspeaker as a flat piston in a rigid infinite baffle, the Kirchhoff-Helmholtz integral reduces to the Rayleigh integral in formula 2.6.

After displacement measurement and acceleration calculation, the acquired data are used to compute the total **Accumulated Acceleration Level (AAL)** and the total **Sound Pressure Level (SPL)** [15, 16, 30, 31, 48, 51].

2.3.1. AAL and SPL computation

Considering the acceleration $A(\omega)$ for each point and using the Rayleigh integral formulation, which is the approximation of Kirchhoff-Helmholtz integral formula [2] under the hypothesis that the loudspeaker vibrates in an infinite rigid baffle and its surface is flat, it is possible to define the sound pressure $p(\omega, r)$.

In fact, starting from the Kirchhoff-Helmholtz integral formula

$$p(\omega, r) = \frac{1}{4\pi} \int_{S_c} \left(j\omega\rho_0 V(\omega, r) \, \frac{e^{-jk|r_a - r_c|}}{|r_a - r_c|} + p_s(\omega, r) \frac{\partial}{\partial n} \frac{e^{-jk|r_a - r_c|}}{|r_a - r_c|} \right) dS_c \tag{2.5}$$

where $V(\omega, r)$ is the sound particle velocity on and normal to the surface S_c and $p_s(\omega, r)$ is the sound pressure on S_c.

By applying the hypothesis of infinite rigid baffle we can notice that $p_s(\omega, r) = 0$ and obtain the Rayleigh integral formulation:

$$p(\omega, r) = \frac{\rho_0}{2\pi} \int_{S_c} \frac{A(\omega, r)}{|r_a - r_c|} \, e^{-jk|r_a - r_c|} \, dS_c \tag{2.6}$$

where:

- $\rho_0 = 1.184 \; [kg/m^3]$ is the standard air density.
- $k = 2\pi f/c$ is the wave number, where $c = 343.21 \; [m/s]$ is the standard sound speed in air.
- r_a is the distance from the cone to the point the SPL is calculated in.
- r_c is the distance between the measured point and the center of the cone (it depends on the measurement grid).
- $e^{-jk|r_a - r_c|}$ is the Green function that takes in account the phase delay due to the distance between the measured point and the listening point where the total SPL is computed.

Besides the pressure, we also need a quantity that describes the total mechanical energy of the loudspeaker but, missing geometrical information and material parameters (such as the Young's Modulus[3] E), it is not possible to calculate the kinetic and potential energy of the mechanical vibrations based on measurement results. In order to define the mechanical energy of the loudspeaker we can use instead the accumulated acceleration $a(\omega, r)$:

$$a(\omega, r) = \frac{\rho_0}{2\pi} \int_{S_c} \frac{|A(\omega, r)|}{|r_a - r_c|} \, dS_c \tag{2.7}$$

[3]Mechanical parameters such as the Young's Modulus are often unknown to the loudspeaker designers because depends on the supplier manufacturing chain and on the manufacturing process to obtain the finished loudspeaker.

The accumulated acceleration $a(\omega, r)$ and the relative Accumulated Acceleration Level AAL is a quantity that does not takes in account the phase of the acceleration and its physical meaning is to represent the ideal maximum total SPL if all the points on the cone surface move in-phase. In fact, AAL is a quantity introduced by Professor Wolfgang Klippel in order to quantify the ideal maximum sound pressure level which could be produced if all points on the radiating surface ideally moved in-phase [31, 32]. In fact, considering the modulus of the acceleration $|A(\omega, r)|$ and neglecting the Green function, it is considering as if the acceleration of all measure points is in-phase. The distance $|r_a - r_c|$ is computed taking into account the position of the i-th point at disrance r_c on the radius and the distance r_a to the reference point where the SPL and the AAL are computed, as shown in figure 2.9.

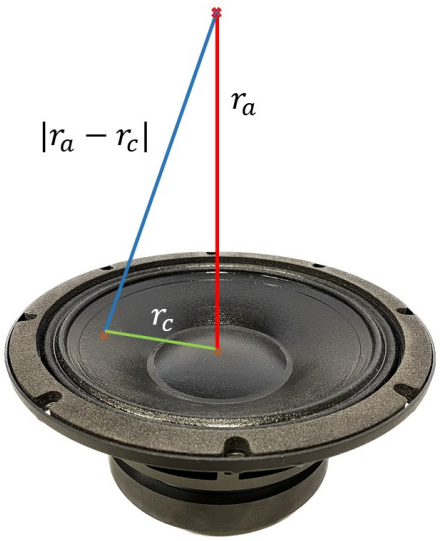

Figure 2.9: Distance between the i-th measured point on the radius at a distnace r_c from the cone center and reference point r_a where AAL and SPL are computed.

After $p(\omega, r)$ and $a(\omega, r)$ computation, it is possible to compute the total Accumulated Acceleration Level AAL and the total Sound Pressure Level SPL as:

$$AAL(\omega, r) = 20 \log_{10} \left(\frac{a(\omega, r)}{\sqrt{2} p_0} \right) \ [dB] \tag{2.8}$$

$$SPL(\omega, r) = 20 \log_{10} \left(\frac{|p(\omega, r)|}{\sqrt{2} p_0} \right) \ [dB] \tag{2.9}$$

where $p_0 = 20 \ \mu Pa$ is the standard sound pressure in air.

In figure 2.10 a comparison plot between AAL and SPL on a 6 inches woofer is shown. Neglecting the technical aspect of the measurement that will be analyzed in detail in chapter 4, we can immediately see how the two curves start to be increasingly different above a certain frequency (the break-up frequency introduced in chapter 2).

Below the break-up frequency, the loudspeaker is in the so called **piston mode regime**: the cone is sufficiently stiff to move as a whole and all the cone parts move in-phase. Above the break-up frequency different vibration modes appear and some parts of the cone start moving out of phase with respect to the others.

This behaviour causes a decrease in the SPL (that, differently from the AAL, takes into account the phase) with respect to the AAL, which supposes all the vibrations contributions are perfectly in phase at the reference point. In the SPL calculation, 2 effects prevent this from happening:

1. Not all parts move together due to the surface modal behaviour.
2. Not all points have the same distance from the reference point: this difference causes phase delay becoming increasingly important with increasing frequency.

Among the two effects, modal behaviour is by far the most relevant one, especially at low frequency. At high frequency, however, distance difference definitely plays a role.

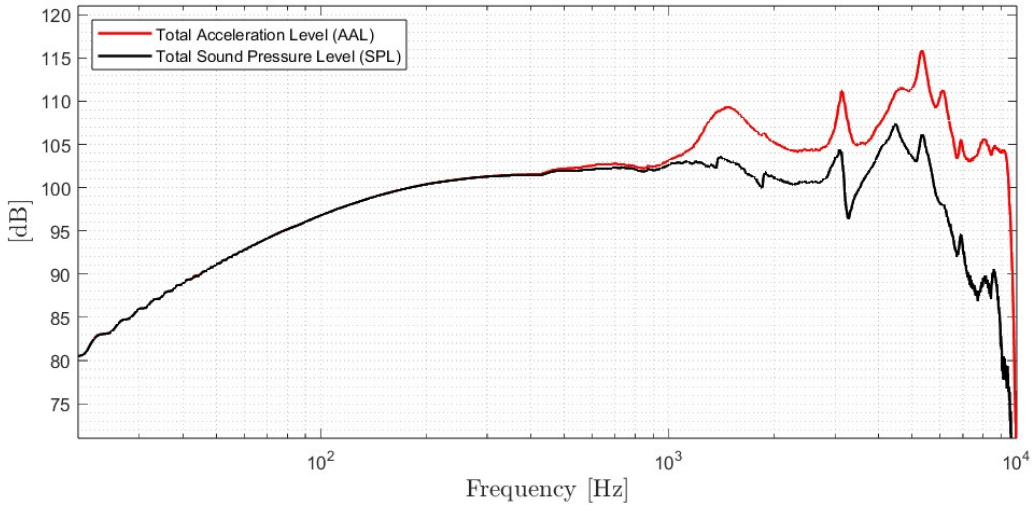

Figure 2.10: Total Accumulated Acceleration Level (AAL) and total Sound Pressure Level (SPL) comparison.

2.3.2. Cone area division for Rayleigh integral computation

In order to compute the Rayleigh integrals 2.6 and 2.7, we need to consider the whole measured surface S_c. Since the outer region of the loudspeaker cone is not moving and does not contribute to radiation, we can discard the last millimeters on the edge. Since we are spatially sampling the cone surface, each measure point has a specific radiating surface associated to it depending on its position.

In figure 2.11 we can see how the relation between a measure point and its portion of the cone area is shown. This area has been calculated by dividing the surface in concentric circular crowns, calculating their area and dividing it for the number of points in each circular crown (that coincides with the number of radii of the grid).

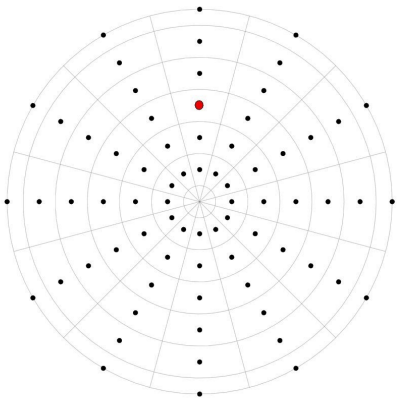

Figure 2.11: Cone area division with respect measurement points.

2.4. In-phase, anti-phase and quadrature components

In addiction to the decomposition in circular and radial modes seen in 1.3.1, a second form of decomposition can be used to identify loudspeaker regions effectively contributing to the total radiated sound pressure level SPL.

Any vibration can be expressed as the sum of three components according to the phase relation with the total sound pressure as calculated in the reference point.

The in-phase component constructively contributes to the total radiated sound pressure, the anti-phase component destructively contributes to sound radiation and the quadrature component does not contribute to sound radiation at all [30].

The total complex cone vibration displacement of each point on the cone surface can thus be decomposed in three components whose relative importance can vary with frequency [52]:

$$x_{total} = x_{inPhase} + x_{antiPhase} + x_{quadrature} \tag{2.10}$$

The phase of the displacement at each point on the surface is set in relation to a reference phase φ_{ref} starting from the phase φ_p of the total sound pressure $p(\omega, r)$ computed with 2.6 and considering both the time delay of the acoustical wave traveling from the cone surface to the observation point and the opposite sign between acceleration an displacement.

The reference phase of the in-phase displacement component for each point on the surface can be calculated as (figure 2.12):

$$\varphi_{ref} = \varphi_p + k|r_a - r_c| + \pi \tag{2.11}$$

where an additional phase shift of π has been added from the phase difference between the displacement and the acceleration of the surface[4].

The vertical displacement on the Z axis of each point of the cone surface expressed in formula 2.10 can be in-phase, in anti-phase or in quadrature giving a different contribution to the total SPL.

In piston mode regime, all the points will move in-phase according with φ_{ref}, so that x_{total} coincides with its $x_{inPhase}$ component contribution on the displacement of formula 2.10.

The more we go up with the frequency and the more there will be points of the cone that will move in anti-phase so in formula 2.10 the $x_{antiPhase}$ component will increase.

[4]Since we are considering the acceleration in the Rayleigh formulation.

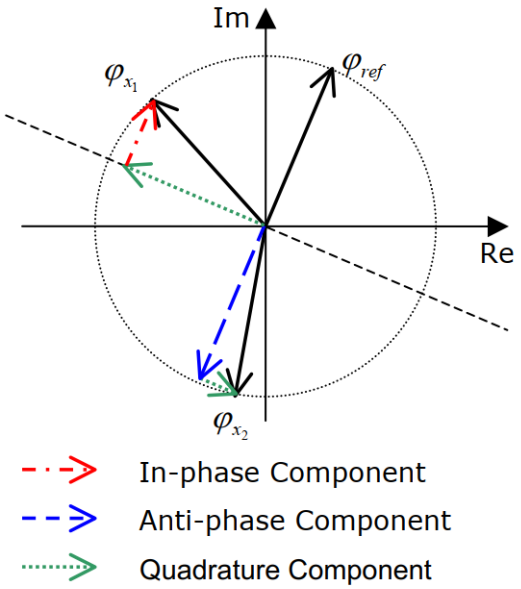

Figure 2.12: in-phase, anti-phase and in quadrature components in phasorial domain [30].

The **in-phase** contribution that describes the positively related component between the phase of the displacement at each point φ_x is defined as:

$$x_{inPhase} = \mathfrak{Re}_+ \left[X(\omega, r) \cdot e^{-j\varphi_{ref}} \right] \cdot e^{j\varphi_{ref}} \tag{2.12}$$

and contributes constructively to the sound pressure. The acceleration level AAL is identical to the SPL assessing the in-phase component only.

The **anti-phase** component is defined as:

$$x_{antiPhase} = \mathfrak{Re}_- \left[X(\omega, r) \cdot e^{-j\varphi_{ref}} \right] \cdot e^{j\varphi_{ref}} \tag{2.13}$$

and contributes destructively to the SPL.

Eventually, the **quadrature** component is defined as:

$$x_{quadrature} = \mathfrak{Im} \left[X(\omega, r) \cdot e^{-j\varphi_{ref}} \right] \cdot e^{j(\varphi_{ref} + \frac{\pi}{2})} \tag{2.14}$$

and it does not contribute to the SPL because the total volume velocity of this component is always zero whereas the AAL of the quadrature component is usually not negligible.

In figure 2.13 we can see instead the three components decomposition for a given measurement point. We can notice the in-phase part is dominant in the lower frequency part because of the piston mode regime.

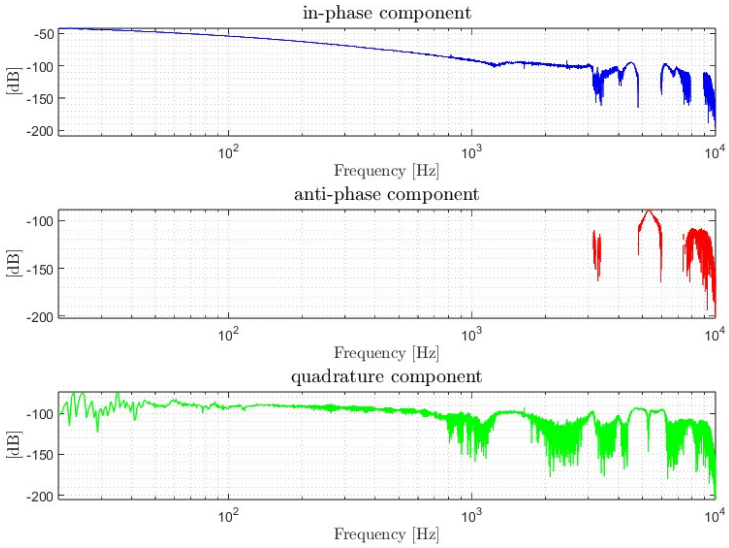

Figure 2.13: In-phase, anti-phase and quadrature components in frequency.

In figure 2.14 we can see the comparison between the *Transfer Function* of a given measurement point and the reconstructed complex displacement according to 2.10 of the same point. As expected, we can notice the two curves coincide.

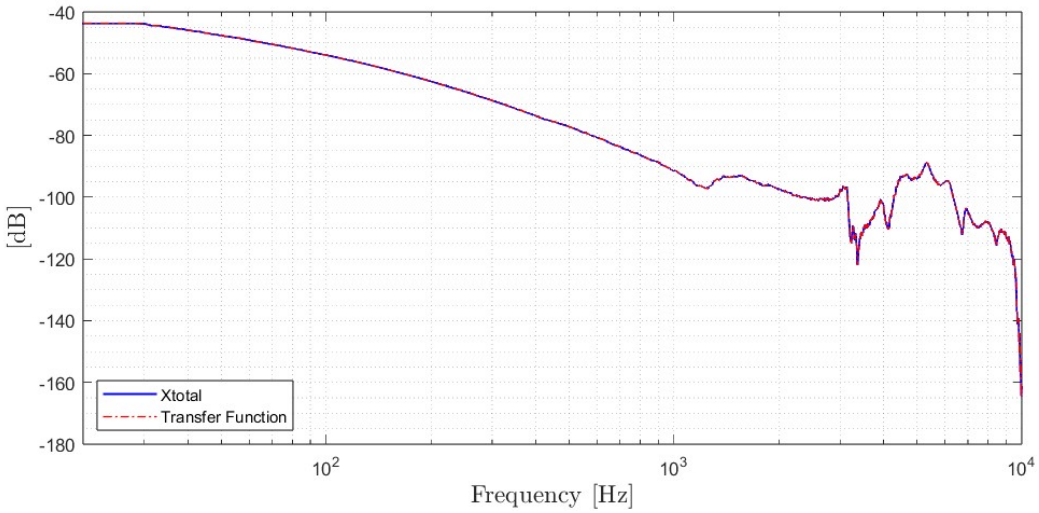

Figure 2.14: Comparison between the Transfer Function of a given measurement point and its complex displacement obtained as $x_{total} = x_{inPhase} + x_{antiPhase} + x_{quadrature}$.

2.4.1. Components AAL and SPL

Once the components has been computed for all the cone surface, it is important to calculate their AAL and the SPL as in section 2.3. We notice that the in-phase and anti-phase AALs are equal to the in-phase and anti-phase SPLs while the SPL calculated considering only the quadrature component is null (as definition implies) [30, 31, 52].
The frequency dependence and the relative importance of the three components give precious information, which can be used to modify the loudspeaker design, improving its acoustic response over the frequency range of interest.
Moreover, we can notice that components AAL and SPL, and in general the components computation is closely related to the total AAL and SPL behaviour due to the relation between the components computation and the phase of the pressure $p(\omega, r)$ computed in 2.6. If the total SPL presents a dip and its distance from the AAL grows, means that there is an acoustical cancellation.
A complete acoustical cancellation generates a zero in the transfer function and, in this case, the in-phase and the anti-phase components have the same AAL. In general, the farther the total AAL and SPL curves are, the closer the in-phase and anti-phase components AAL and SPL curves are to each other. If we consider the total AAL and SPL plot in figure 2.10, we can see the corresponding components decomposition AAL and SPL plot in figure 2.15 and we can notice how the in-phase and anti-phase curves are closer at the frequencies where the AAL and SPL in figure 2.10 are further away. Finally, we can also notice both the quadrature and the anti-phase AAL-SPL components are not present below the cutoff frequency, as the loudspeaker still is in piston mode regime.

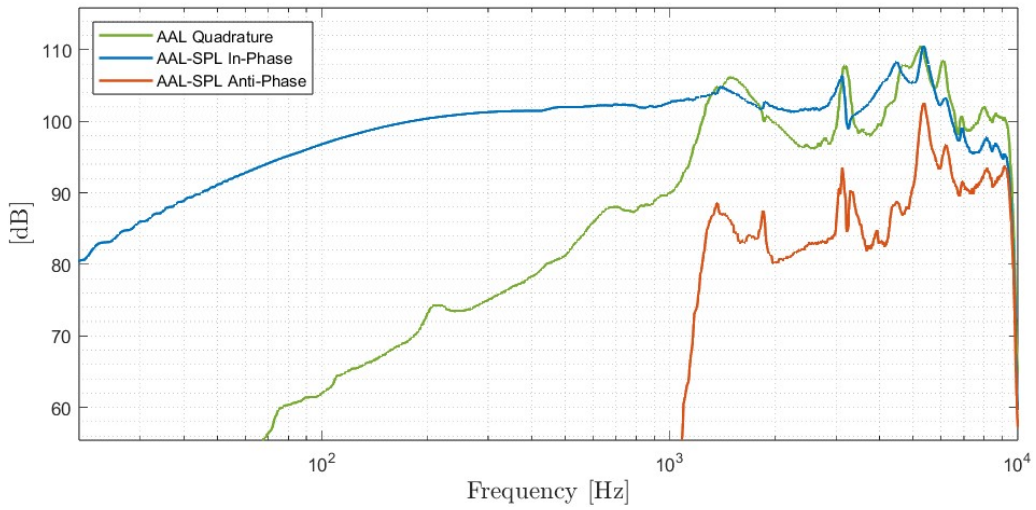

Figure 2.15: Components AAL and SPL realated to the same loudspeaker total AAL and SPL measured in figure 2.10.

2.4.2. Components graphical visualization

Another important and extremely useful information we can obtain from the components computation is to understand what are the parts of the cone that are in-phase, in anti-phase or in quadrature at a given frequency.

According with [52], the real part of the components can be represented and plotted considering the whole surface or over a specified cone radius or diameter. The visualization of the components on the loudspeaker cone profile is extremely useful for loudspeaker designers in order to immediately understand which are the parts of the cone in anti-phase destructively contributing to the total SPL.

In figure 2.16 we can see an example of the real part of the components at 300 Hz (on the top), 1500 Hz (in the middle) and 5000 Hz (at the bottom) plotted along a cone diameter.

We can notice how the components contribution changes with frequency:

At 300 Hz the loudspeaker is moving in piston mode regime, all the points are moving in-phase with respect to the voice coil displacement and the anti-phase component is null.

At 1500 Hz some points in the loudspeaker cone and on the surround suspension start moving in anti-phase causing a negative contribution to SPL. Since these plots are related to the AAL and SPL in figure 2.10 (and therefore to the components plotted in figure 2.13), we can see that SPL is actually lower than AAL at that frequency.

At 5000 Hz a more complex behaviour begins and several parts of the cone on the surround and on the dust cup are moving in anti-phase. In fact, in figure 2.10 we can see a dip in the SPL curve around this frequency caused by this anti-phase behaviour.

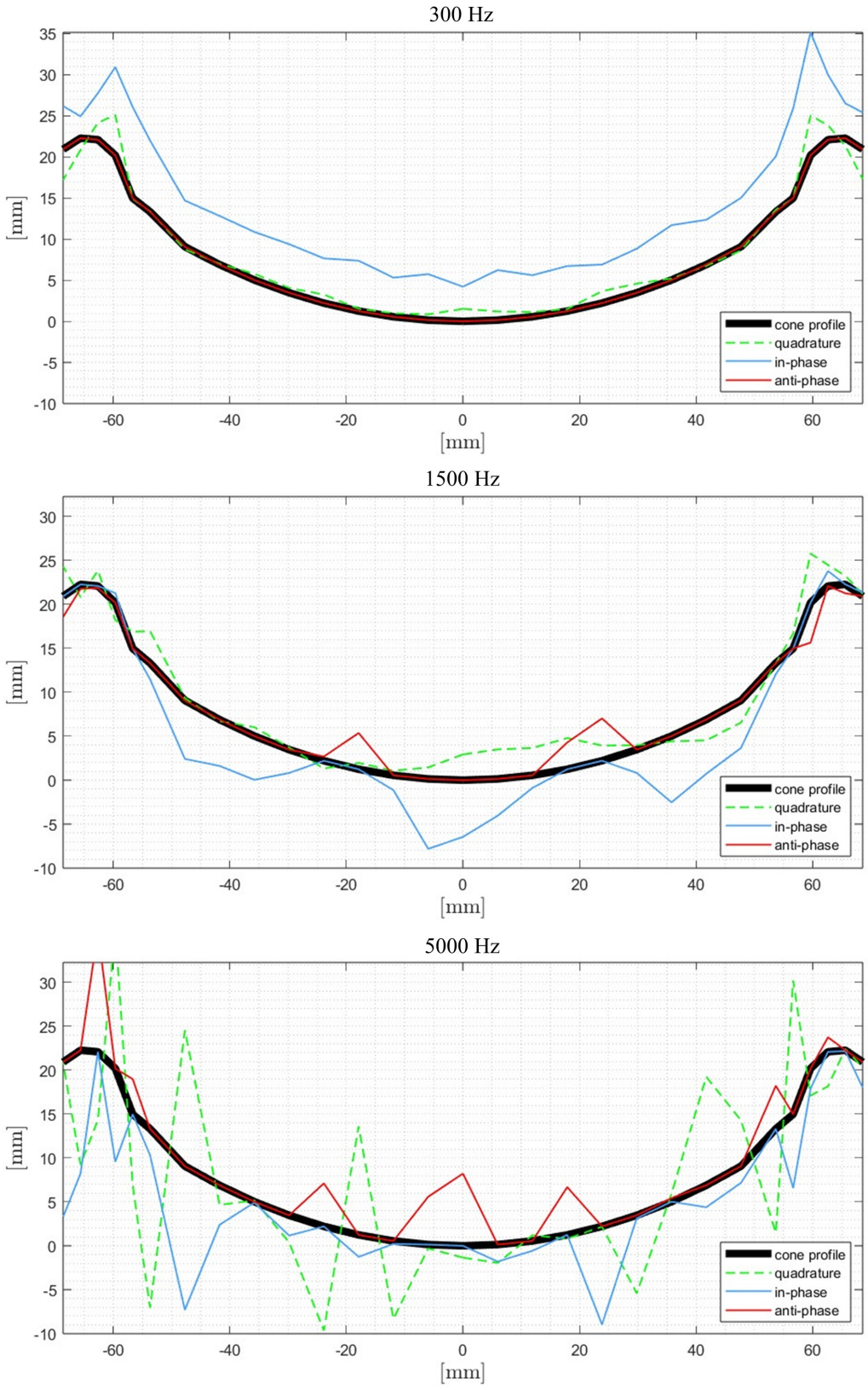

Figure 2.16: Components real part plot along a 6 inches cone diameter at 300 Hz on the top, 1500 Hz in the middle and 5000 Hz at the bottom.

3 | Laser scanning technique for loudspeaker cone vibration measurement

3.1. Working principle and experimental setup

After analyzing the usefulness of having a measurement instrument that can characterize the behaviour of a loudspeaker membrane and explaining the main theoretical concepts behind it, we will now analyze the structure of the machine and its implementation highlighting the critical points and the strong points.

The instrument design is inspired on [41, 42] but the idea is to make it more flexible, reliable, economical and customizable. Instead of designing a dedicated mechanical structure including dedicated motors and mechanical constraints, an **EPSON Scara T3** industrial robot [53] has been used. This choice makes the instrument much more customizable and the robot can also be dedicated and used for other purposes as well.
The operating principle is moving a laser on a cone surface according to the points of a grid, defined in section 2.2.2, and, by properly varying the distance between the laser and the surface so that the distance from the sensor always falls into the measurable range, using it to acquire a measurement of displacement for each grid point. The stimulus signal (section 2.2.1) that generates the cone vibration is generated in MATLAB and is then amplified before being sent to the loudspeaker. The acquisition is carried out by connecting the laser sensor output to a sound card and reading the output voltage value from it. Both acquisitions and signals post processing are performed in MATLAB.
Finally, the computed total SPL using 2.6 and 2.9 is compared with an SPL measurement performed in anechoic room with a microphone placed at 1 meter on the loudspeaker axis. Although we do not expect the computed total SPL to coincide with the measured with a microphone one, this step is useful to check the correctness of both the computed SPL behaviour and of the considered pressure phase to calculate the components in section 2.4 [48].

Figure 3.1: SPL measurement in anechoic room with a free-field pressure microphone. The loudspeaker is placed in a closed box that is an approximation of the infinite rigid baffle where acoustic short circuit is not present. As explained in in section 2.3, Rayleigh total SPL computation refers to an infinite baffle response where acoustic short circuit is not taken into account. Not being the box infinitely extended, some deviation between the measured and calculated SPL is expected.

3.1.1. Power and signal routing

To sending the stimulus signal and to recording the laser sensor output signal a **MOTU M4** sound card has been used setting the sampling frequency at 48000 Hz and the buffer size at 1024 samples. In order to compensate latency, a cross-correlation in post processing has been used, as explained in section 2.2.1. Since measurements are acquired, stored and processed as double precision variables (that corresponds to 64 bit floating point .wav files), whose representation interval is between 1 and -1, a sound card calibration is required to rescale the laser output to a proper value expressed in millimeters. The sound card calibration has been performed sending to the sound card input a sinusoidal signal of known amplitude and recording the digital representation in MATLAB. Repeating this procedure for different amplitudes, the whole amplitude range of the sound card input can be calibrated and the relation between input signal voltage and the recorded digital amplitude can be established.

Sound card calibration was required to rescale digital recorded values (acquired, stored and processed as double precision 64 bit floating point variables with $[-1; 1]$ representation interval) to a proper value in mm for the laser displacement sensor output signal. At the end of the calibration process a sound card *calibration constant* is found.
Moreover, the MATLAB code is also able to read the sound card input during the robot movement between two grid points. In order to know when the robot needs to move the laser displacement sensor in a different position (and thus when it is time to send a new stimulus to the loudspeaker and to acquire its displacement), an an easily detectable impulsive movement along the vertical axis is imposed to the robot whenever the sensor needs to be moved from one point to another. This signal is used in the MATLAB code as a trigger signal to start a new measure sending the stimulus to the amplifier and recording the laser output during the cone vibration.
The amplifier used is a **Powersoft K20** without any DSP setting, a 0 dB output attenuation and 32 dB gain. The sound card is connected to the amplifier with an XLR cable and the amplifier is then connected to the loudspeaker with a speakon-faston power cable. In order to measure and correctly set the amplifier output voltage, a **Fluke 289** multimeter has been used. The multimeter is connected to the amplifier output before starting the measurement to measure and set the desired voltage RMS.
The amplifier output voltage settings depends on many factors such as the loudspeaker nominal impedance, the loudspeaker size and its parameters but, in general, having an higher output voltage RMS gives a better SNR. In this work output voltages between 10 and 30 V_{RMS} have been used. This voltage range also ensure a constant voice coil temperature during the measurement.

Figure 3.2: Amplifier output RMS voltage measurement with a Fluke 289 multimeter.

3.1.2. Loudspeaker preparation and mechanical constraints

The loudspeaker is fixed on an horizontal surface with a **mandrel** in order to avoid undesired structural vibrations and to have a fixed central reference point for the measurement grid.

The cone surface is treated with a white **3D scanning powder** in order to improve light reflection and consequently the laser signal to noise ratio. Several tests have been performed and a better SNR is obtained whenever a white measured surface is used.

Other treatment materials have been tested, such as face powder and white paint but the added mass or the grains of dust crumbling and flying through the laser beam make the measurement unreliable.

Figure 3.3: Loudspeaker cone treated with white 3D scanning powder.

In order to attach the laser sensor to the robot arm, a **3D printed bracket** has been realized starting from a customized **Solidworks** CAD drawing. The laser sensor has been fixed to the bracket using two screws and bolts.

The laser sensor-bracket system must be configured as external tool in the EPSON RC+ robot software [53, 54].

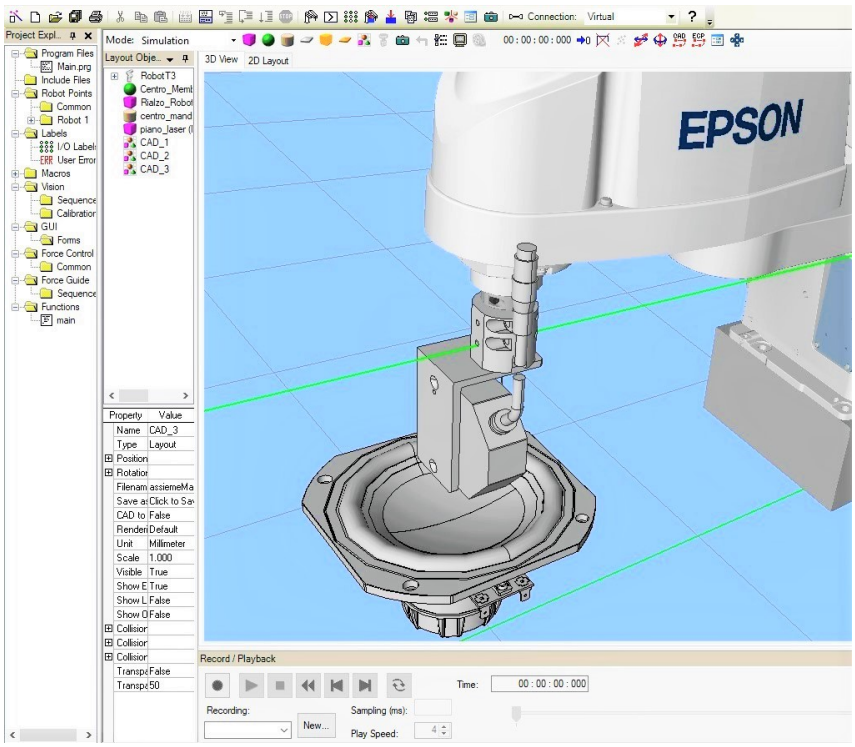

Figure 3.4: EPSON RC+ 7.0 software robot simulator with the laser-bracket system attached to the robot arm.

3.1.3. MATLAB framework

MATLAB is the software used both for the measurement phase and for the post processing phase. Since there is no a direct communication between MATLAB and the robot, and the timing to start a new acquisition in different grid points is given by the trigger signal from sound card as discussed in section 3.1.1.

MATLAB framework is divided in four scripts and two functions:

1. The `"Measure Data"` script, which must be executed both in the measurement phase and in the post processing phase, has the following features:
    - It reads an Excel .xlsx file where the user inserts parameters such as loudspeaker diameter, sampling frequency, initial and final sine sweep frequencies and measurement grid type.
    - It creates the measurement folders directory where all the measurements and data are stored.
    - Generates the sine sweep stimulus signal according with section 2.2.1 and it saves it as .wav file.

- It generates the measurement grid according to section 2.2.2 generating its X, Y and Theta coordinates in .txt files which can be directly uploaded on the EPSON robot script. A specific function that creates the grid, saves the coordinates and creates also the radius coordinate vector for each measured point, later used in the post processing phase.
- It generates and saves a .txt datalog file with all the measurement parameters and settings using a dedicated external function.

2. The `"Measure Framework"` script is used to perform displacement measurements on the grid points and to store the .wav files of each measurement from the sound card. This script uses the variables generates in the `"Measure Data"` script and has the following features:
   - After detecting all the connected audio devices, it creates a graphical user interface where the user can select the desired input and output channels.
   - In order to calibrate and set the desired amplifier voltage output, it generates a single tone at 500 Hz for several seconds. At this step the loudspeaker is not connected to the amplifier yet, the user can connect the multimeter to the amplifier output to check the voltage value.
   - It performs a single test measurement where also noise floor is acquired. Noise floor is recorded acquiring the laser sensor signal when no stimulus is applied to the loudspeaker. In this step the measurement SNR is computed and a plot containing both the measured displacement and noise floor FFT is shown to the user.
   - It performs automatic measurements according to the number of points in the grid (see section 2.2.2). In this step the code communicates with the input and output sound card channels, waits for the trigger input signal defined in section 3.1.1 and starts the acquisition sending the stimulus to the amplifier and recording from the sound card input at the same time. Eventually all measured displacements are saved as .wav files in a subfolder of the measurement directory.
3. The `"Measure Import"` script is the first post processing step. The aim of this script is to read, load and prepare measured data for the AAL, SPL and components computation presented in chapter 2.

This script:

- Reads the .wav files stored from laser displacement measurement as double variables and loads them in a matrix where each row corresponds to a single point measurement.
- Computes the inverse filter and performs the convolution operation in order to obtain the *Transfer Function impulse response* $h(t)$ according to section 2.2.1 and with [45, 47]. All the impulse responses are stored in a matrix.
- Starting from Impulse Responses, it computes both the voltage to displacement and voltage to acceleration *Transfer Function* for each measurement point as explained in section 2.2.3. A *Transfer Function* matrix and an acceleration matrix are stored to be used in AAL, SPL and components calculation.
- Plots all the processed signals (displacement in time, IR, acceleration etc.) for each measured point.

4. The `"Measure Post Processing"` script uses processed data from `"Measure Import"` to perform the calculation explained in section 2.3 and 2.4. This script:
   - Properly defines the distance between measured points and the reference point for SPL computation[1] and stores them in a vector.
     A comparison between SPL calculation using CAD geometry and a "flat disk" surface approximation for the radiating surface is presented in chapter 4.
   - Computes the cone area vector for each measured point as explained in section 2.3.2.
   - Performs the Rayleigh integrals for total AAL and SPL computation according with section 2.3 and plots the results.
   - Performs and plots the in-phase, anti-phase and quadrature components and then computes their AAL and SPL as explained in section 2.4.
   - Plots the components on a cone radius according to section 2.4.2.

The MATLAB post processing phase (including the `"Measure Import"` and the `"Measure Post Processing"` scripts elaboration) can last from 5 to 40 minutes depending on the number of measured points of the grid, on the sampling frequency and on the time of each single measurement.

[1] SPL and AAL are computed in a reference point of 1 meter on loudspeaker axis as in figure 2.9.

3.1.4. Laser Doppler Vibrometer

The used laser head model is **Keyence LK-G32** with a 655 nm emission. The laser sensor controller, needed for a proper signal conditioning, is connected to an external 24 V power supply. The sensor focal range is ± 5 mm, the output is set to ± 10 V and it is connected to the sound card input via XLR cable.

The laser sampling frequency is set to 50 kHz and no moving average filter is used. In order to increase the SNR, a $2V/mm$ scaling constant is set into the controller.

Keyence **LK-Navigator** software is used to set the laser controller parameters and check the head distance from the loudspeaker cone surface.

Figure 3.5: Keyence LK-G32 laser head.

Since the laser must be kept in a certain distance from target surface to perform the measurement, the robot must move the laser sensor along the Z axis according to the loudspeaker cone profile. Since the EPSON software, the laser software and MATLAB does not communicate each other, programming the robot to behave as explained was a very challenging part of this work. A solution was found calculating the Z axis coordinate of the robot starting from the loudspeaker CAD drawing.

Another important aspect that we have to take into account is that laser could have some problems in measuring points along the cone surface that are in an almost vertical position. When the laser can not properly detect the triangulated light signal on its lens. In order to avoid it, the laser must be oriented so that the movement is always in the radial direction and the laser always stays parallel to the loudspeaker edge. For this reason, the laser orientation must change for every radius (depending on the grid type) and the angular coordinate Theta must be sent to the robot to to vary the position of arm 4 (where the laser sensor-bracket system is attached) at each radius.

3.1.5. EPSON Scara T3 Robot

The machine used to move the laser on the grid points is an **EPSON Scara T3 robot**. This is a 4 joints robot ensuring both maximum precision and a practical way to perform the measurement [53].

Figure 3.6: EPSON Scara T3 robot.

Differently from the machine proposed in [41, 42], the loudspeaker remains fixed to the mandrel and the robot moves the laser sensor over the grid points.

The robot is coded in **EPSON SPEL+** language on the **EPSON RC+ 7.0** software [54, 55] to perform the movements. The RC+ software reads and loads into vectors grid XY coordinates, the laser angle rotation coordinate Theta and the laser Z axis coordinate from .txt files. Each point where the robot moves is defined by the coordinates X, Y, Z, Theta.

The movement time between different points is defined by the user and it must be at least 1.5 times the length of the stimulus defined in section 2.2.1 to ensure that MATLAB does not start performing the measurement during the robot movement. At every robot movement, an impulsive signal triggers to the sound card, allowing MATLAB to start the measurement, as explained in section 3.1.1.

4 | Analysis of results

4.1. Analyzed loudspeakers

In order to test the measurement instrument, two 6 inches (152 mm) loudspeakers have been used as test samples. Both the loudspeakers share the same identical components and design except the spider, which in one case is stiffer.

In fact, looking at the Thiele-Small parameters, they are all almost identical except for the mechanical stiffness of the suspensions ($K_{MS} = 2.65\ N/mm$ for the more compliant loudspeaker and $K_{MS} = 5.65\ N/mm$ for the stiffer one).

Figure 4.1: CAD drawing of the analyzed loudspeaker model.

This loudspeaker has a single roll surround made of rubber and a reversed dust cup. Both loudspeakers were treated with white 3D scanning powder (as explained in section 3.1.2) and a decrease in noise floor level of up to 5 dB was achieved. In figure 4.2 we can see the differences between SPLs measured in a closed box (as in figure 3.1) of both loudspeakers. They have a very similar behaviour: small differences start to be observed after 2000 Hz. It can also be observed that lodspeaker with a stiffer spider has a response that drops off faster after 5000 Hz due to the greater stiffness of the suspension.

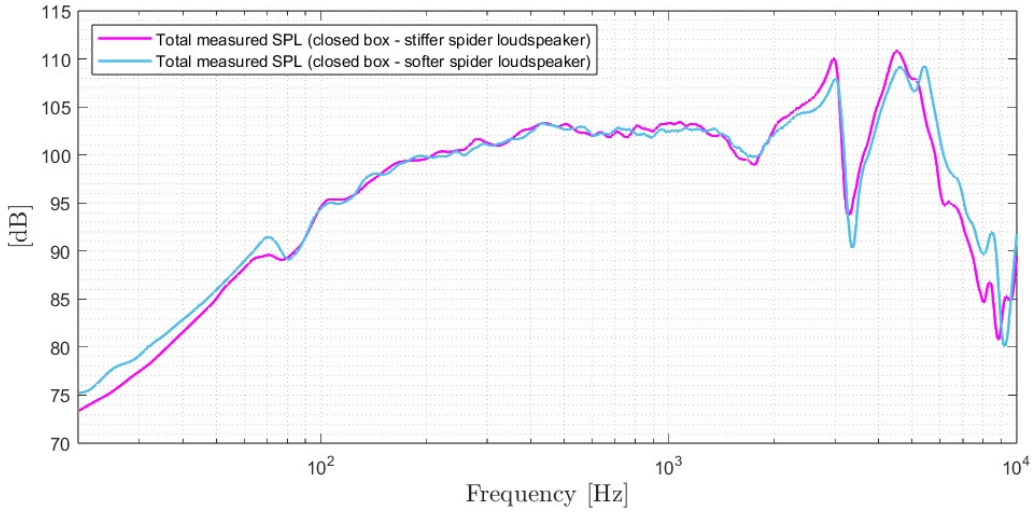

Figure 4.2: Closed box measured SPLs for loudspeakers equipped with stiffer and softer spider.

4.2. Measurement data and setup

Since the tested loudspeakers are used as mid-low frequency drivers, frequencies in the 10 Hz - 10000 Hz have been analyzed. All measurements lasted 5 seconds and several grids layouts have been tested.

For the stiffer loudspeaker, all 4 grids in figures 2.5, 2.6, 2.7 and 2.8 have been used for measurements.

For the more compliant loudspeaker, two measurement were performed, one with the grid in figure 2.6 and one with another grid pattern with 792 measurement points on 22 radii (36 points for each radius with 2 mm constant spacing).

Results from these measurements have been compared with those obtained using the commercial instrument machine [41, 42].

Loudspeaker cone shape plays an important role in the AAL and SPL computation (and therefore in in-phase, anti-phase and quadrature components computation). Since Rayleigh integral formulas for pressure and accumulated acceleration 2.6, 2.7 take into account the distance between the measurement point and the reference point as in figure 2.9, cone geometry becomes important to compute the $|r_a - r_c|$ quantity.

During the design phase, an ideal drawing of the loudspeaker is created in CAD in software such as SolidWorks.

Due to components tolerances and various aspects in the assembly process, the geometry of the actual loudspeaker can differ from that of the ideal CAD model[1].

In order to take into account the real shape of the cone, a laser scan of the surface should be performed, as foreseen in the commercial machine [41]. Since the sound card used for this work cannot record DC signals (such as the one that laser displacement sensor would output while scanning the loudspeaker surface), the geometry from the ideal CAD drawing was used to perform all the calculations.

Moreover, pressure and accumulated acceleration calculation has been performed also considering the cone as flat surface and neglecting its real shape[2].

4.3. Measurement results

In this section, the different measurement results for each loudspeaker are presented. For each measurement both the cone as flat surface approximation and the cone as ideal surface from CAD geometry (figure 4.1) were considered.

In the following figures we can also immediately notice the difference between the SPL computed with Rayleigh integral 2.6 and the SPL measured with a microphone in a closed box (figure 3.1). Especially at low frequencies (where the loudspeaker is in piston mode regime and acoustic short circuit in free air measurement occurs), is shown a different behaviour: measured SPL has a non linear behaviour and it is lower with respect to the calculated one. This phenomena occurs because Rayleigh integral formula calculate the SPL in an ideal infinite baffle, while the closed box in the anechoic room is not ideal and thus its measurement response have some irregularities.

All the measurement results on the two loudspeakers will be compared and commented later in section 4.5.

[1] There could be some differences depending on the materials, gluing points and small manufacturing irregularities.

[2] This analysis has been performed in order to compare the results in different cases and to study the differences between them.

4.3.1. AAL and SPL computation varying the radii number

In this section is shown how AAL and SPL change in function of the number of radii we are taking into account (and consequently changing the total number of measurement points). This analysis is important to show the difference in the results considering different grids. In figures 4.3 and 4.4 is shown AAL and SPL curves variation depending on the number of radii under analysis. It is possible to notice how the curves become more detailed around the "critical points" where resonances and antiresonances occur as the number of radii under analysis increase. Obviously, a change in AAL and SPL corresponds to a change in the frequency behaviour of the components too.

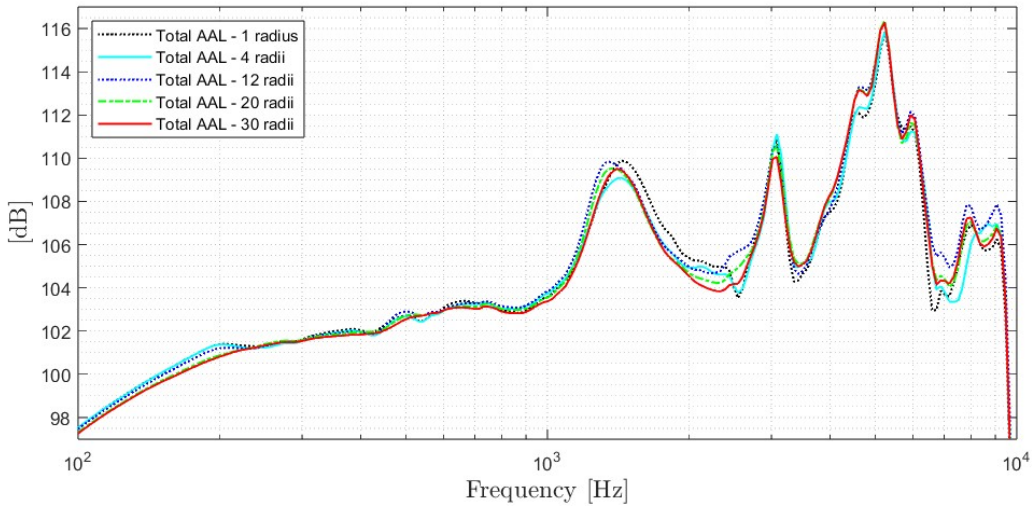

Figure 4.3: AAL variation depending on the considered number of radii.

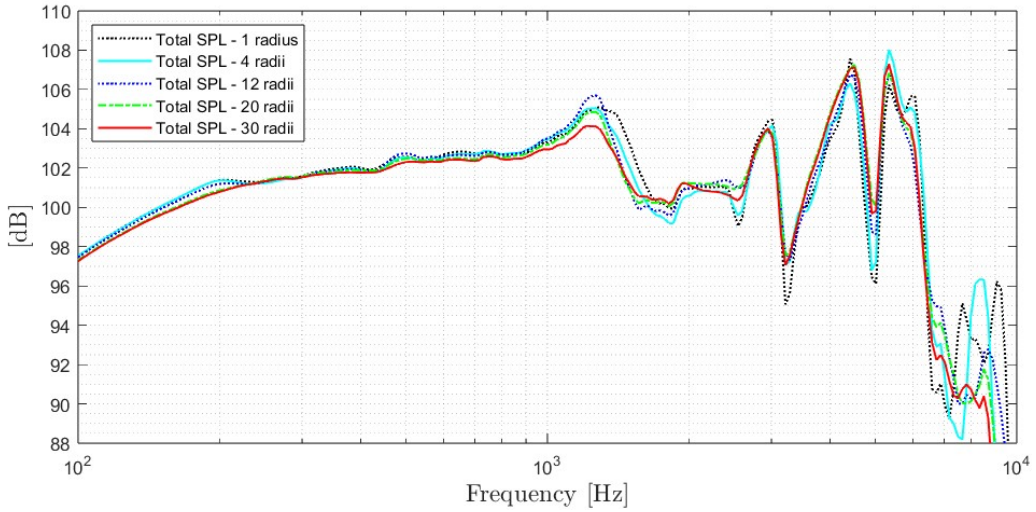

Figure 4.4: SPL variation depending on the considered number of radii.

4.3.2. Loudspeaker equipped with a stiffer spider ($K_{MS} = 5.65\ N/mm$)

We start the result analysis by looking at the loudspeaker equipped with the stiffer spider.

AAL and SPL in figure 4.5 and components calculation results in figure 4.6 refer to a 450 measurement points grid with constant radius spacing (figure 2.5).

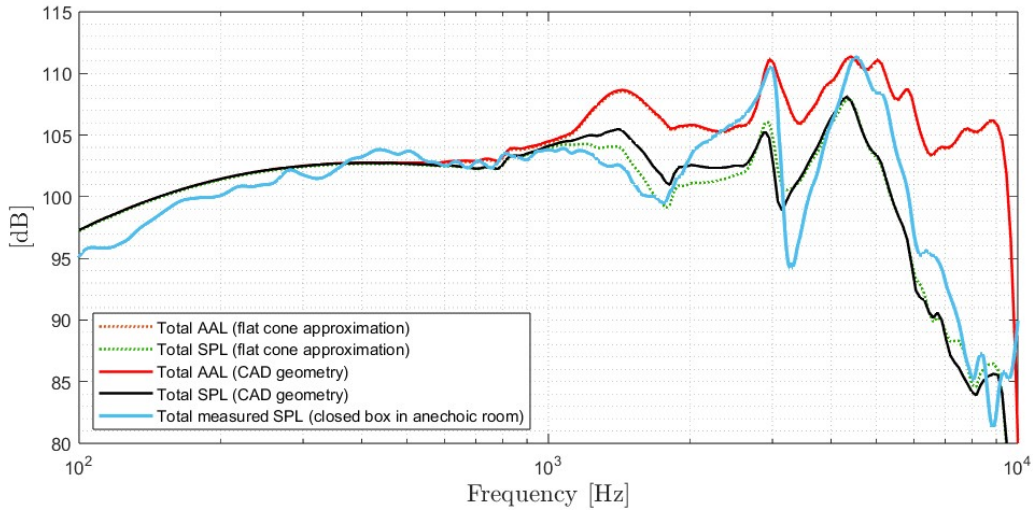

Figure 4.5: AAL and SPL curves of the stiffer spider loudspeaker for a 450 measuring points grid with constant spacing on the radius.

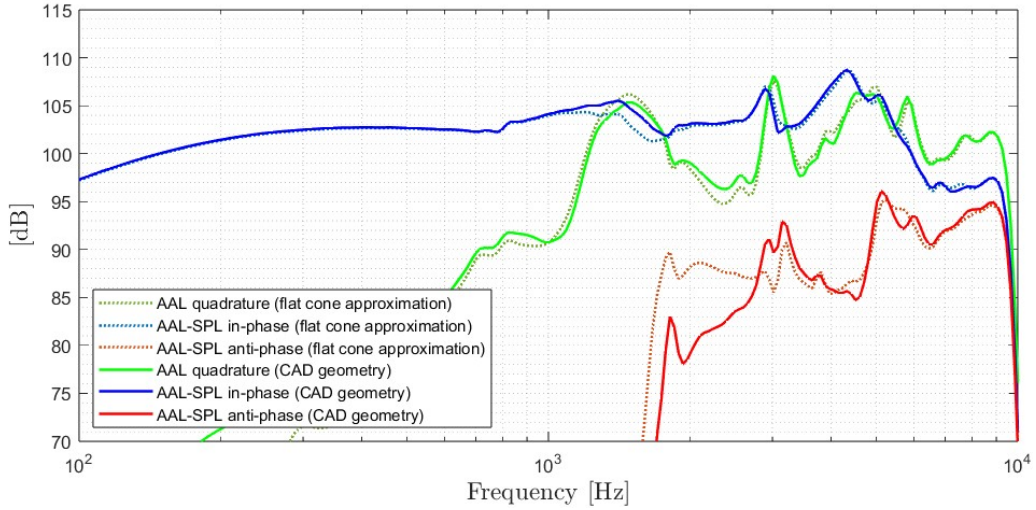

Figure 4.6: In-phase, anti-phase and quadrature components of the stiffer spider loudspeaker for a 450 measuring points grid with constant spacing on the radius.

Figures 4.7 and 4.8 show AAL and SPL and components calculation results for the 450 measuring points grid with non constant radius spacing (figure 2.6).

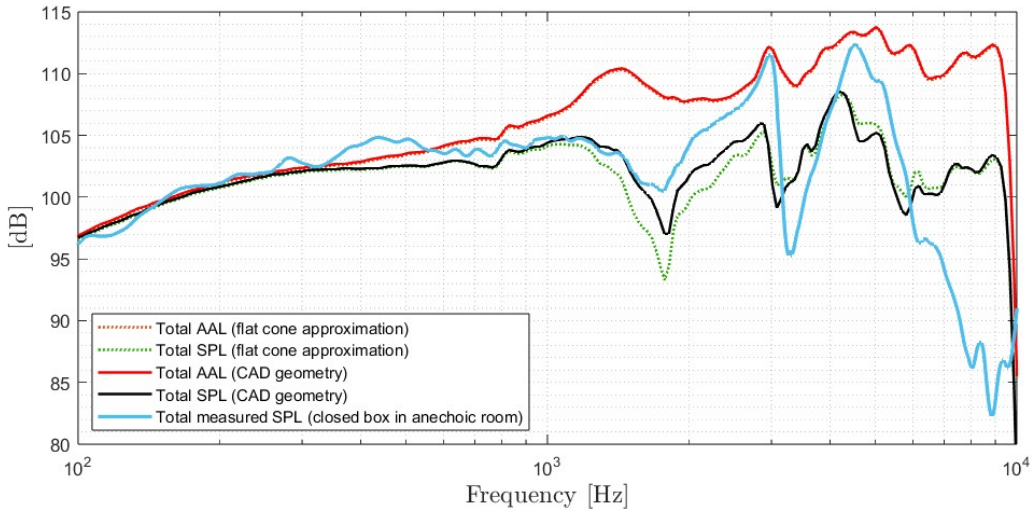

Figure 4.7: AAL and SPL curves for a 450 measuring points grid with non constant points spacing on the radius (higher points density on the edge) for the loudspeaker equipped with the stiffer spider.

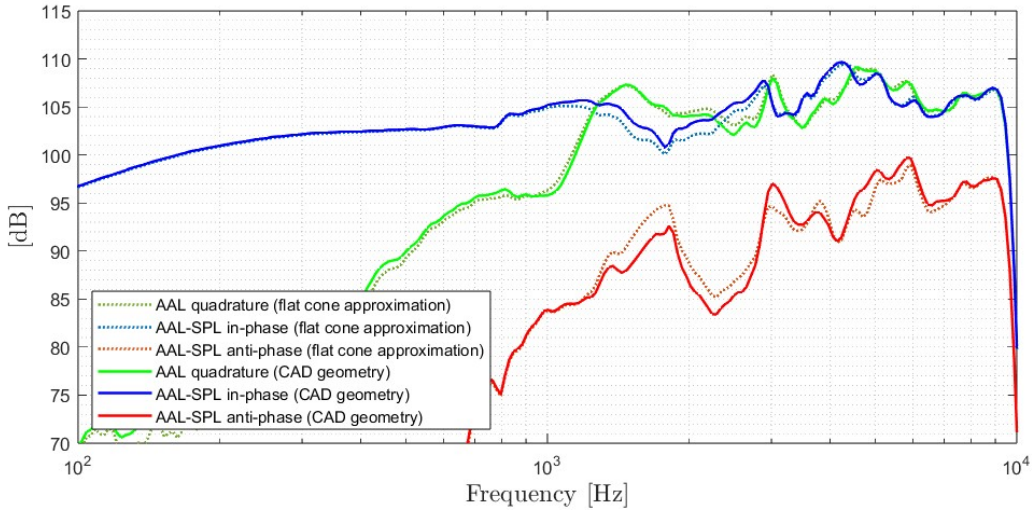

Figure 4.8: In-phase, anti-phase and quadrature components of the loudspeaker equipped with the stiffer spider for a 450 measuring points grid with non constant points spacing on the radius (higher points density on the edge).

Figures 4.9 and 4.10 show AAL and SPL and components calculation results for the detailed scan grid with 3200 measuring points grid with constant radius spacing (figure 2.7).

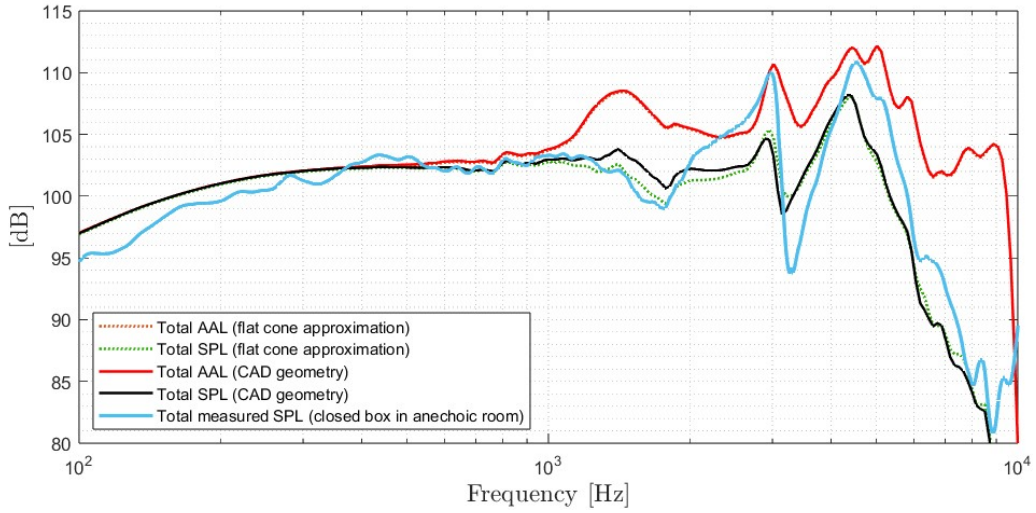

Figure 4.9: AAL and SPL curves for a 3200 measuring points grid with constant points spacing on the radius for the loudspeaker equipped with the stiffer spider.

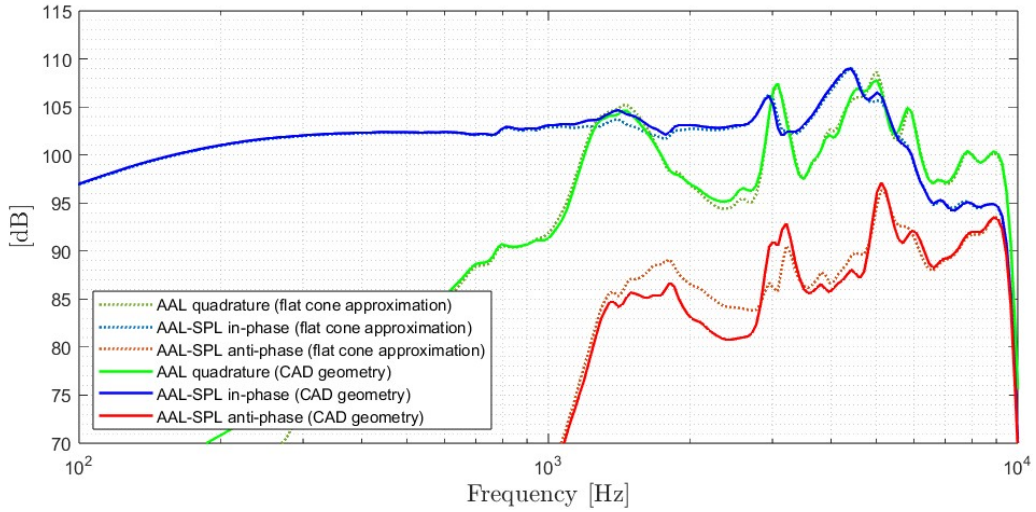

Figure 4.10: In-phase, anti-phase and quadrature components for the loudspeaker equipped with the stiffer spider for a 3200 measuring points grid with constant points spacing on the radius.

Lastly, figures 4.11 and 4.12 show AAL and SPL and components calculation results for a 3200 measuring points grid with non constant radius spacing (figure 2.8).

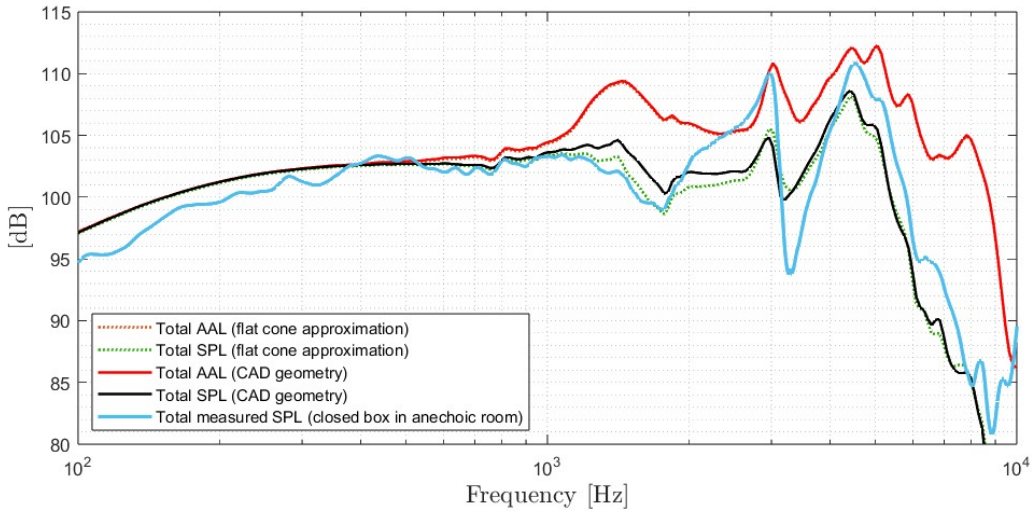

Figure 4.11: AAL and SPL curves for a 3200 measuring points grid with non constant points spacing on the radius (higher points density on the edge) for the loudspeaker equipped with the stiffer spider.

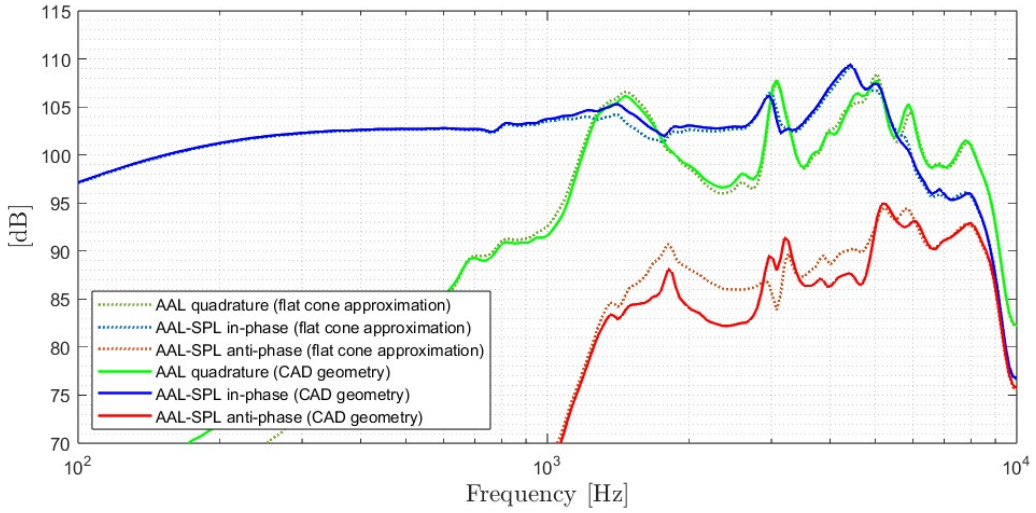

Figure 4.12: In-phase, anti-phase and quadrature components for a 3200 measuring points grid with non constant points spacing on the radius (higher points density on the edge) for the loudspeaker with the stiffer spider.

4.3.3. Loudspeaker equipped with a softer spider ($K_{MS} = 2.65\ N/mm$)

Figures 4.13 and 4.14 show AAL and SPL and components calculation results for a 450 measurement points grid with non constant points spacing on the radius (higher points density on the edge) of the measurements preformed on the loudspeaker with equipped with a softer spider.

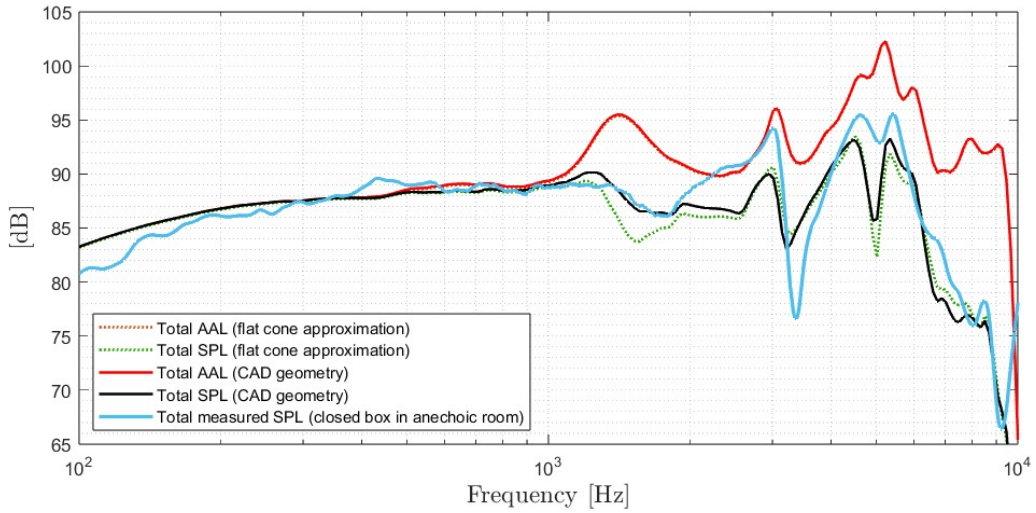

Figure 4.13: AAL and SPL curves for the 450 measuring points grid with non constant points spacing on the radius (higher points density on the edge) for the loudspeaker equipped with the softer spider.

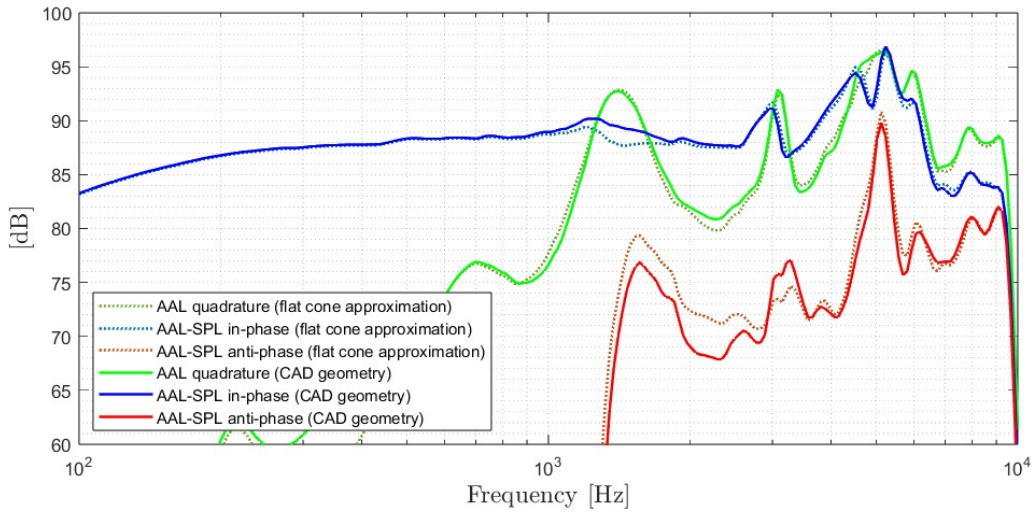

Figure 4.14: In-phase, anti-phase and quadrature components for the loudspeaker equipped with the softer spider for a 450 measuring points grid with non constant points spacing on the radius (higher points density on the edge).

Figures 4.15 and 4.16 show the AAL and SPL and components calculation results for the 792 measurement points grid. This grid has 22 radii and 2 *mm* constant spacing among measurement points on each radius.

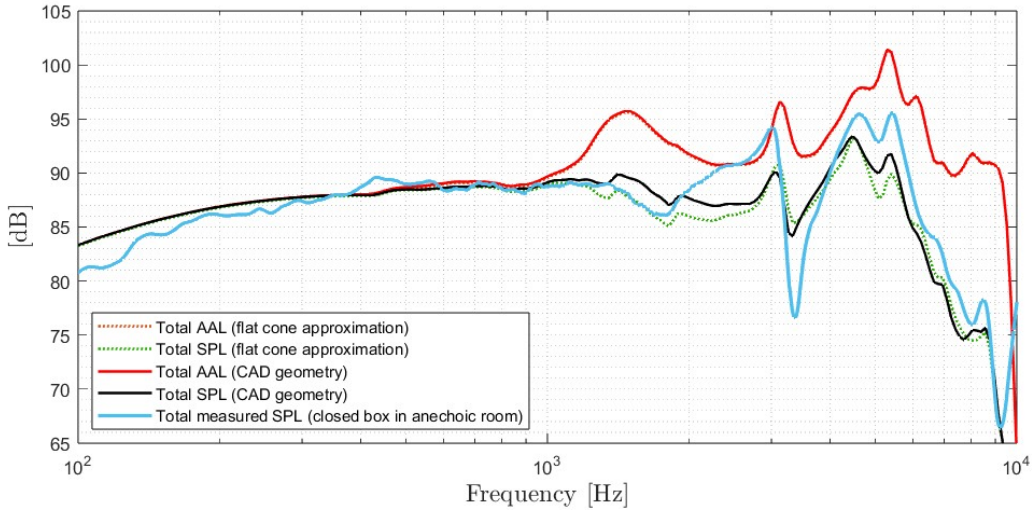

Figure 4.15: AAL and SPL curves for a 792 measuring points grid with constant points spacing on the radius and 22 radii (36 measurement points spaced 2 *mm* on each radius).

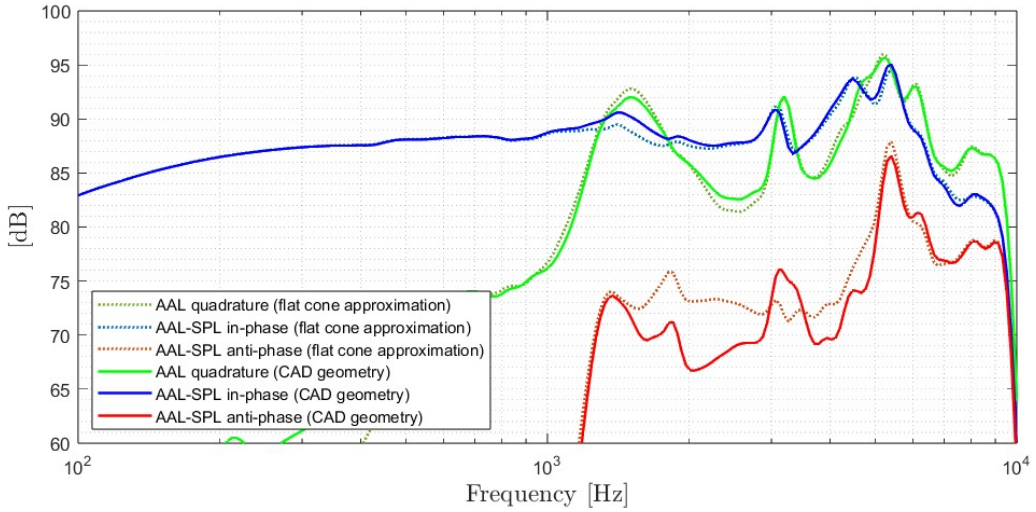

Figure 4.16: In-phase, anti-phase and quadrature components for the loudspeaker equipped with the softer spider for a 792 measuring points grid with constant points spacing on the radius and 22 radii (36 measure points spaced 2 *mm* on each radius).

4.4. Results comparison between the experimental measurement system and the commercial laser measurement instrument

The measurements results of the loudspeaker with the softer spider have been compared with the ones of the Klippel instrument machine [41, 42]. Results of this comparison are shown in this section and some comments on them are presented in section 4.5.

To compare the results obtained with the Klippel hardware as closely as possible with those obtained with the in-house developed instrument, a 451 measurement points grid was used to perform the scan with the Klippel hardware and a 450 measurement points grid with non constant points spacing on the radius (higher points density on the edge) as in figure 2.6 was used to perform the scan with the in-house developed instrument.

Please, note that some differences could not be eliminated and should be taken into account in the following analysis:

- In the commercial hardware grid distance among measurement points decreases as radius increases (following an $1/r$ relation), while the in-house developed instrument distance among measurement points is constant (though reduced and become denser above a certain radial coordinate).
- The commercial hardware considers the real cone geometry in its calculations while the in-house developed instrument, as already explained, at the current stage retrieves loudspeaker geometry from the ideal CAD model (no flat cone surface approximation was used for this comparison).

Figure 4.17 shows the comparison between the AAL as computed with the Klippel hardware machine and as computed with the in-house developed instrument.

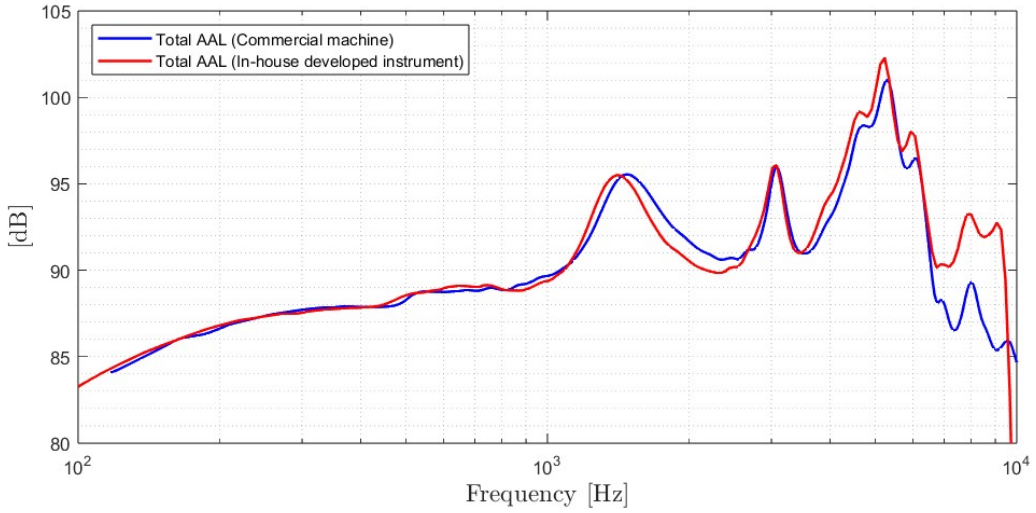

Figure 4.17: AAL results comparison between the Klippel machine (with a 451 points grid) and in-house developed instrument (with a 450 points grid).

Figure 4.18 shows a comparison between the SPL as measured in an anechoic room placing a microphone at 1 m distance, with the loudspeaker in the closed box (as shown in figure 3.1), SPL as computed with the commercial hardware and with the in-house developed instrument.

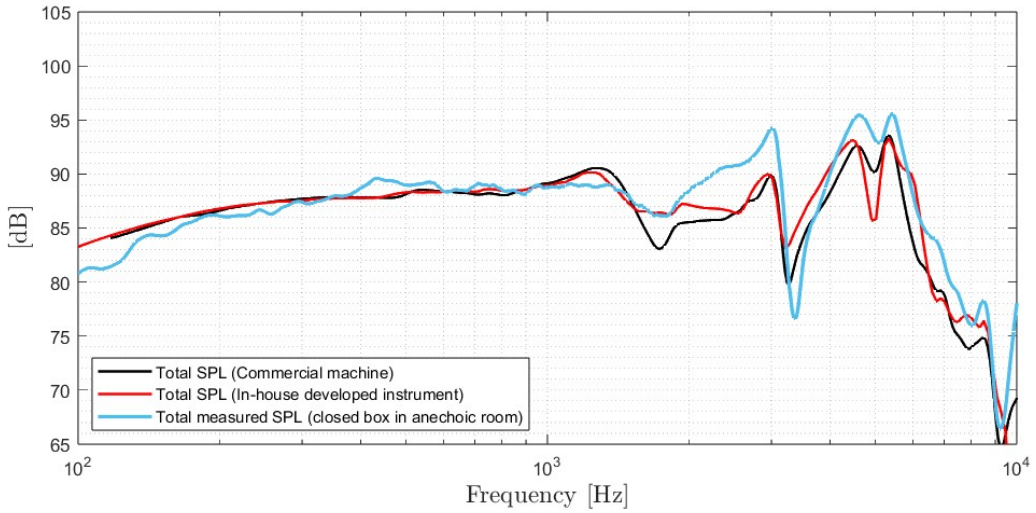

Figure 4.18: SPL results comparison between the Klippel machine (with a 451 points grid) and in-house developed instrument (with a 450 points grid). The blue curve is the SPL measured in an anechoic room placing a microphone at 1 m distance, with the loudspeaker in the closed box (as shown in figure 3.1).

Figure 4.19 shows the the comparison between the components computed with the Klippel hardware and with the in-house developed instrument.

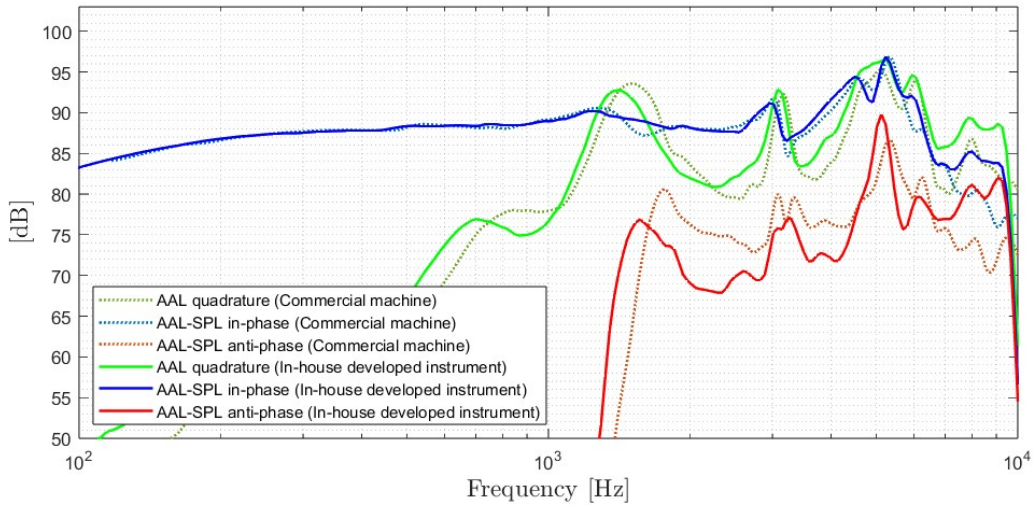

Figure 4.19: Components results comparison between the Klippel hardware (with a 451 points grid) and the in-house developed instrument (with a 450 points grid).

4.5. Comments on results

The first interesting result is that AALs of the flat cone surface approximation and CAD geometry surface coincide for each different measurement grid.

This was an expected result because, since AAL does not takes into account the phase, the distance between the measured points and the observation point $|r_a - r_c|$ does not affect the phase[3].

Another important observation we can made is how the SPL calculated starting from the CAD geometry generally fits better the SPL measured with the microphone in a closed box. Measurements performed with detailed grids (figures 2.7 and 2.8) show better agreement with the measured SPL than measurements performed with exploratory grids (figures 2.5 and 2.6) do.

This proves the importance of having a denser grid to account for geometrical details. Another important aspect relating to the grid choice is the spatial distribution of measurement points on the radius. We can notice an antiresonance in the SPL around 1800 Hz in both loudspeakers.

[3]The small variations of the distance $|r_a - r_c|$ due to the differences between the CAD geometry and the real profile of the cone still influence the phase in a negligible way.

Decomposing the vibrational behaviour in a modal summation following the analysis performed on [16], we can suppose behaviour at that frequency depends on the rubber surround that is oscillating in anti-phase with the other parts of the surface (and therefore gives a negative contribution to the SPL). We can see how in grids with a denser number of measurement points on the edge, the calculated SPL at that frequency shows better the measured one (for example in figures 4.5 and 4.7).

To summarize the results on the loudspeaker with the stiffer spider, the following figures compare the AALs and SPLs calculated for the four different measurement grids considering the flat cone profile and CAD geometry approximation. We immediately notice that the AALs are almost identical to the previously discussed observations.

Furthermore, in the case of both the exploratory grid and the detailed grid, a higher density of measurement points at the edge allows for a higher level of precision around the points where resonances and antiresonances occur.

The measurement made with the exploratory grid and the non constant radius spacing differs from the others: even if the problems of the anti-phase behaviour are evident, the measurement was performed with a low SNR and thus AALs and SPLs curves differ greatly from the others, especially at high frequencies.

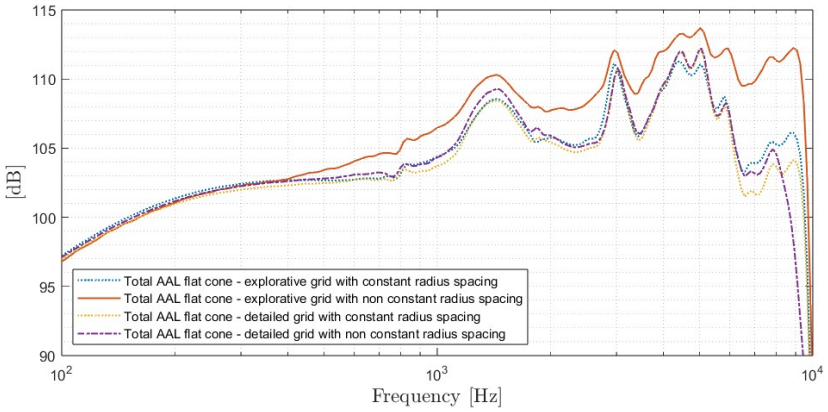

Figure 4.20: AALs comparison between different measurement grids (figures 2.5, 2.6, 2.7 and 2.8) considering flat cone approximation.

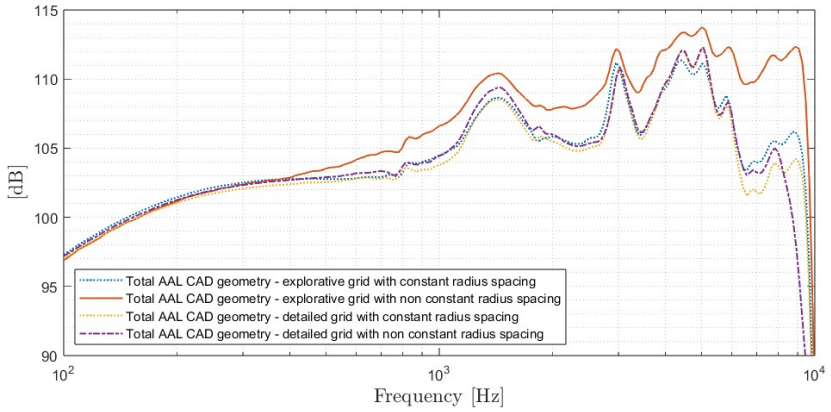

Figure 4.21: AALs comparison between different measurement grids (figures 2.5, 2.6, 2.7 and 2.8) considering CAD geometry.

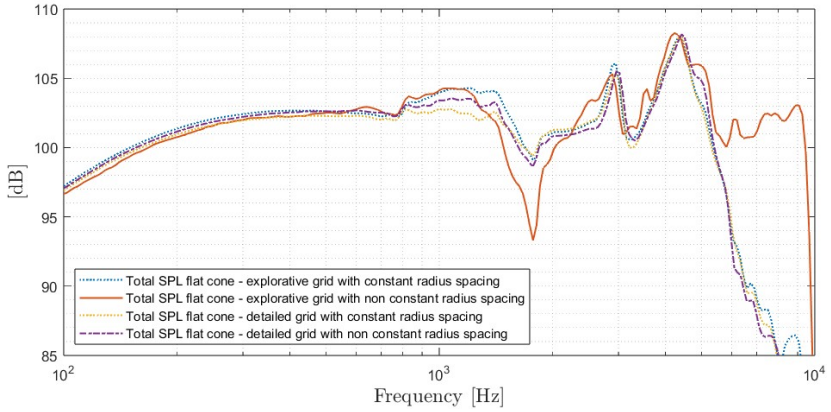

Figure 4.22: SPLs comparison between different measurement grids (figures 2.5, 2.6, 2.7 and 2.8) considering flat cone approximation.

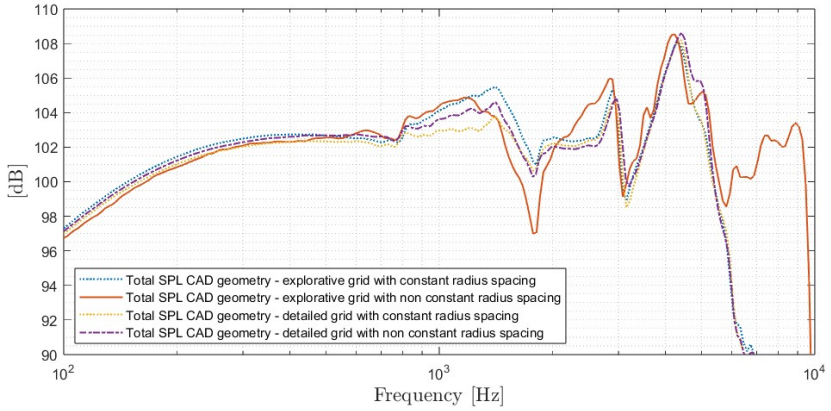

Figure 4.23: SPLs comparison between different measurement grids (figures 2.5, 2.6, 2.7 and 2.8) considering CAD geometry.

The same condition can be retrieved from the analysis of the loudspeaker equipped with the softer spider: the computed SPL shows a better agreement with the measured SPL curve at 1800 Hz (antiresonance frequency) with the exploratory 450 points grid with non constant radius spacing (figure 4.13) with respect to the 792 points grid with a regular radius spacing (figure 4.15). In the components decomposition figures, the anti-phase component appears only above a certain frequency. Since components are strictly related to the AAL and SPL behaviour, as explained in section 2.3 and 2.4, if the SPL computed with the flat cone surface approximation differs from the SPL computed considering the CAD geometry, then components calculated basing on this or that approximation differ too. Looking at the comparison between the commercial hardware and the in-house developed instrument results, the AALs curves are almost identical. The small differences between them can be caused by several factors such as:

- Different SNR in the measurement (especially at high frequencies where displacement is limited).
- Different loudspeaker measuring position that could not be properly centered.
- Since both compared grids have 30 radii at 12 degrees each, the two measurements could be performed on a different rotation angle and thus considering different radii with a slightly different modal behaviour.
- Different post processing filtering and elaboration.

SPL curves are very close too. Both curves follow the profile of measured one. The biggest differences between the two computed SPL curves appears at the "critical points" where resonances and antiresonances occur. Taking also in account the same considerations made for the AALs differences, the SPLs differences can also be caused by:

- Phase difference at the reference point where AAL and SPL are computed considering the real (with its irregularities) or the "ideal" CAD geometry in the calculations.
- Phase difference due to the sound card latency. As explained in section 2.2.1, this latency is compensated only during the post processing step with MATLAB `finddelay` function and taking a known measured IR as reference for the cross-correlations. In this way, small phase delays in the measured displacement due to the real loudspeaker behaviour could have been erroneously compensated as if they come from the sound card.

Both the curves from the Klippel measurement instrument and from in-house developed instrument exhibit a similar behaviour. The differences between them depend on the different AAL-SPL relations, as previously explained.

4.5.1. Components visualization comparison

According with section 2.4.2, after computing the in-phase, anti-phase and quadrature components it is possible to visualize them on the loudspeaker surface by considering their real part [52]. Considering figure 4.18 and fixing the frequency at 5000 Hz where a dip in the SPL is visible in results obtained both with the Klippel hardware and with the in-house developed instrument, we will now compare the components decomposition results.
It must be kept in mind that results can greatly differ depending on the diameter of the loudspeaker we are considering. In particular, there may be the possibility that the grid radii measured with the commercial instrument may not be placed at the same angle as those measured with in-house developed instrument, thus giving a different result.

Moreover, the component plots amplitude is arbitrarily assigned in order to more easily visualize moving parts. In figure 4.24 we can see the components decomposition result of the Klippel instrument for a radius placed at +216 degrees with respect the first one (in the exploratory grid with 30 radii, the corresponding diameter at this angle takes in account the fourth and the eighteenth radii).

Looking at the anti-phase component (on the top), we can notice that the points where the diaphragm is moving in anti-phase lie on the surround and on the dust cup. From the in-phase component plot (in the middle) we can see that the in-phase moving points lie on the cone and on the dust cup surface. The quadrature contribution (on the bottom) is instead spread all over the cone surface.

In figure 4.25 we can see the component decomposition of in-house developed instrument at the same frequency for a radius that is placed at +180 degrees with respect the first one (in the exploratory grid with 30 radii, the corresponding diameter at this angle takes in account the first and the fifteenth radii). We can see in the anti-phase component plot (on the top) that point moving in anti-phase are very close to the ones identified by the commercial instrument. Also the in-phase component plot (in the middle) presents several similarities with the one of the Klippel instrument. The quadrature component (on the bottom) is the one that most differs from the one obtained with the Klippel instrument, although, since in both cases it extends over the entire loudspeaker surface.

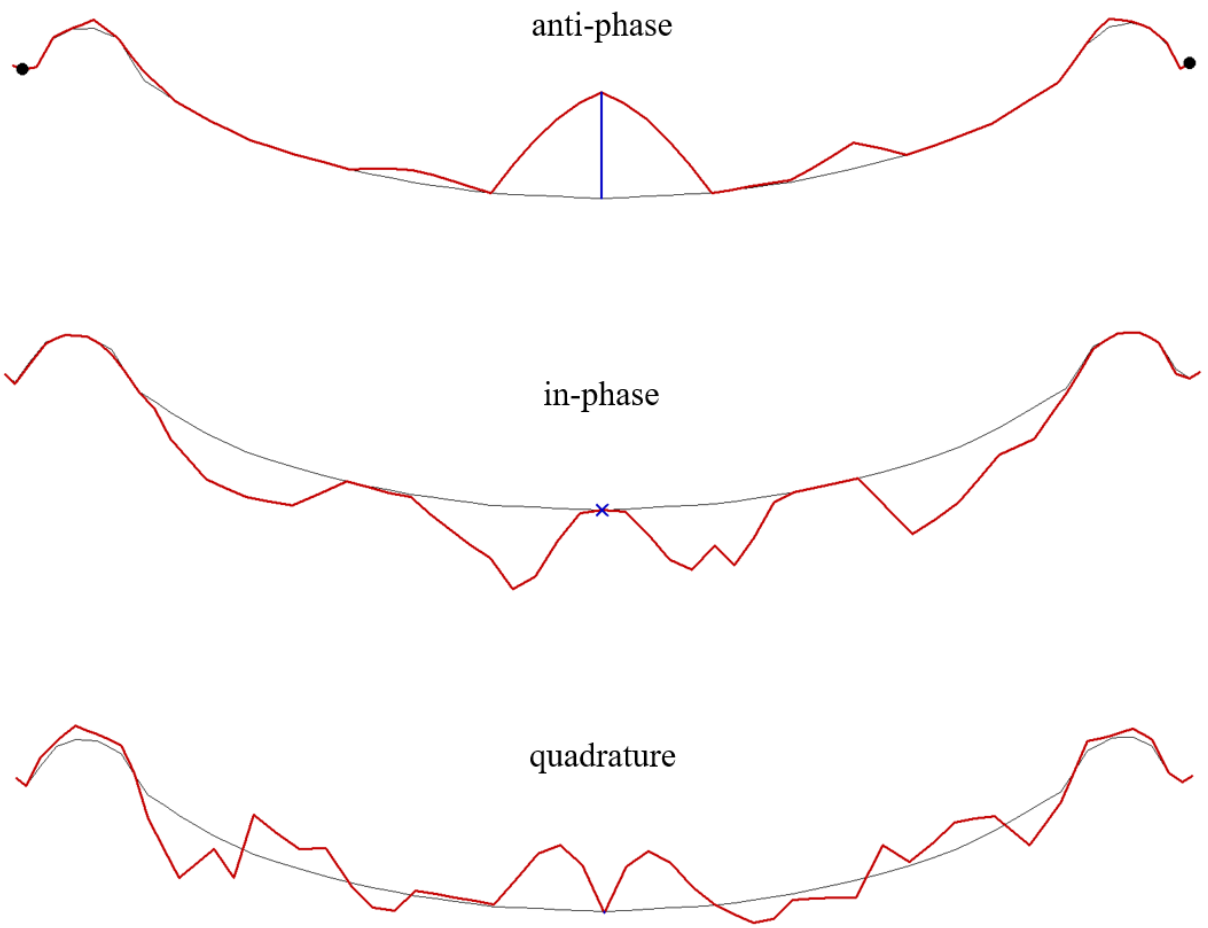

Figure 4.24: Components graphical decomposition results from the Klippel instrument measurement and software at 5000 Hz. Anti-phase component on the top, in-phase component in the middle and quadrature component at the bottom [41].

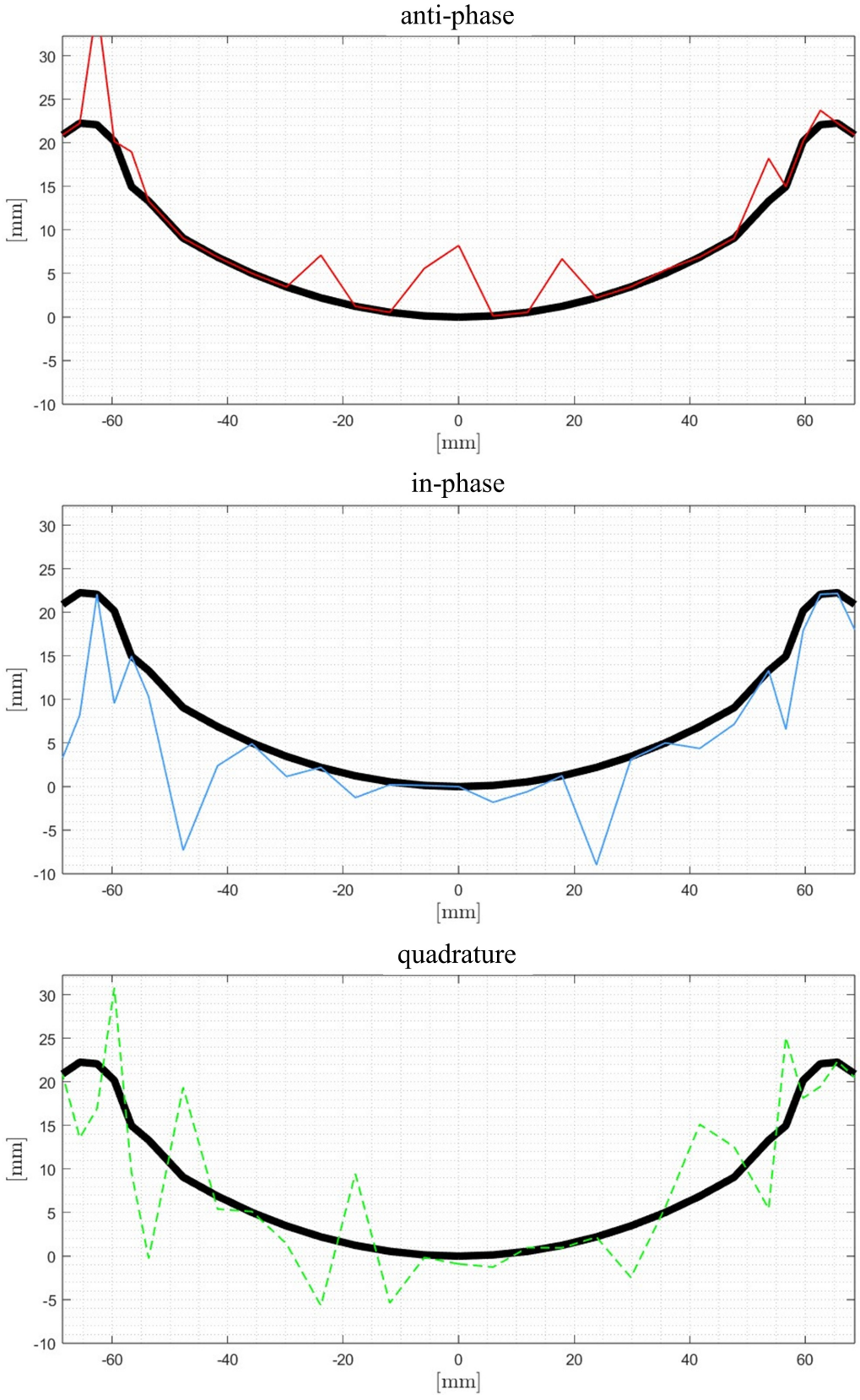

Figure 4.25: Components graphical decomposition results from in-house developed instrument at 5000 Hz. Anti-phase component on the top, in-phase component in the middle and quadrature component at the bottom.

5 | Further developments and conclusions

5.1. The importance of the laser scanning technique in loudspeaker design

The primary objective of this project was to develop a practical and useful instrument that would assist loudspeaker designers in their work. Laser displacement sensors have gained significant popularity over the years and are commonly used in commercial measuring devices. The key emphasis of this endeavor was to demonstrate how vital information for research and development of new products can be derived from a straightforward laser measurement. By harnessing the capabilities of this instrument, hundreds of measurements could be effortlessly executed, eliminating the need for time-consuming manual operations. Moreover, the gathered data could be processed using advanced algorithms and analytical techniques, enabling comprehensive analysis and interpretation.

The significance of this work extends beyond the mere creation of an instrument. It serves as a testimony to the transformative potential of laser measurements in generating crucial insights and supporting the advancement of loudspeaker design. By showcasing the extraction and processing of essential data through this innovative approach, the project aimed to highlight the broader possibilities that exist in utilizing laser instruments for research and development purposes. The successful implementation of this instrument has the potential to help the loudspeaker design process, making it more efficient and streamlined. By automating measurements and employing data processing techniques, designers can gain deeper insights into the performance and characteristics of their products. This, in turn, facilitates the research and development of new and improved loudspeaker designs, leading to enhanced sound quality and user satisfaction.

The use of simulation and prediction software (such as COMSOL) in loudspeaker design has been gaining momentum over the past five years, giving rise to new challenges.

Materials characterization in order to obtain correct simulation results plays an increasingly crucial role. In most cases, the characteristics of materials purchased from suppliers (located especially in South East Asia) are unknown. An hardware such as the one presented in this work is therefore of great use for the characterisation of material parameters.

The possibility of estimating material parameters such as density and Young's modulus by comparing the results of the laser measurement and those of the simulation software opens up a new scenario in the world of loudspeaker design and opens up new possibilities for designers.

Furthermore, the instrument presented in this work could become a turning point and greatly speed up loudspeaker design process. The ability to decompose the vibrational behaviour of a loudspeaker cone and graphically visualize which parts have problems provides the designer with fast and accurate information on how to remedy them.

5.2. Future developments

Several improvements and changes can be implemented to improve the results and reliability of this measurement instrument:

1. An acquisition card or similar hardware with DC-coupled inputs which is able to read the DC voltage from the laser sensor output could be implemented. In this way, two operations could be performed:

   (a) The real cone surface shape could be obtained by calculating the laser sensor distance from the cone surface depending on its output voltage. The real surface shape could then be used to calculate the Rayleigh's integrals 2.6, 2.7 more accurately (instead of using CAD geometry shape).

   (b) Check when the laser sensor goes out of its focal range of measurements and, in case, sending a voltage signal to a robot input port to modify the laser sensor Z axis coordinate.

   This card could be easily controlled in MATLAB and implemented in the already existing framework.

2. The measurement and compensation of the sound card and system latency can be done in the measurement phase instead of in the post processing phase. Using the same MATLAB `finddelay` function introduced in section 2.2.1, the measured displacement signal could be immediately compared with the stimulus signal that is acquired by creating a loop between an output channel and an input channel of the sound card. In this way, only the latency of the sound card and the system are compensated with no risk of compensating delays due to other causes (such as band-limited physical behaviour of loudspeaker components). Another possible approach may be to eliminate or make the measurements latency constant by finding another suitable acquisition device.

3. Once the latency is properly compensated, multiple measurements can be taken at the same measurement point and averaged to greatly improve the SNR.

4. Components graphical visualization (section 2.4.2) on the cone surface can be improved by adding a time dependence (and thus looking at how the components change over time). The total displacement and its time dependence can be implemented and shown on the cone profile too.

5. A 3D total displacement and components displacement decomposition over the loudspeaker surface could be shown as in the [25] work.

Bibliography

[1] Peter G. Craven. Practical adaptive room and loudspeaker equalizer. *AES - 92nd convention*, 1992.

[2] Leo Beranek and Tim Mellow. *Acoustics - Sound Fields, Transducers and Vibration*. Academic Press, 2019.

[3] Wolfgang Klippel. Loudspeaker nonlinearities – causes, parameters, symptoms. *Commun. ACM*, 2019.

[4] David Bie. Vibration resonances of a titanium loudspeaker diaphragm. *AES - 104th convention*, 1998.

[5] Steven L. Garrett. *Understanding Acoustics*. Springer, 2020.

[6] Richard H. Small. Direct-radiator loudspeaker system analysis. *AES journal - Volume 20, number 5*, pages 383–395, 1972.

[7] Richard H. Small. Closed-box loudspeaker systems - part 1: Analysis. *AES journal - Volume 20, number 10*, pages 798–808, 1972.

[8] Richard H. Small. Closed-box loudspeaker systems - part 2: Synthesis. *AES journal - Volume 21, number 1*, pages 11–18, 1973.

[9] Richard H. Small. Vented-box loudspeaker systems - part 1: Small-signal analysis. *AES journal - Volume 21, number 5*, pages 363–372, 1973.

[10] Richard H. Small. Vented-box loudspeaker systems - part 2: Large-signal analysis. *AES journal - Volume 21, number 6*, pages 438–444, 1973.

[11] Richard H. Small. Vented-box loudspeaker systems - part 3: Synthesis. *AES journal - Volume 21, number 8*, pages 635–639, 1973.

[12] Richard H. Small. Vented-box loudspeaker systems - part 4: Appendices. *AES journal - Volume 21, number 7*, pages 549–554, 1973.

[13] Wolfgang Klippel. Measurement of large-signal parameters of electrodynamic transducer. *www.klippel.de*, 2019.

[14] Scott Laurin and Karl Reichard. Determining manufacture variation in loudspeakers through measurement of thiele-small parameters. *AES - 125th convention*, 2008.

[15] Wolfgang Klippel and Joachim Schlechter. Distributed mechanical parameters describing vibration and sound radiation of loudspeaker drive units. *AES - 125th convention*, 2008.

[16] William A. Cardenas. Modeling of higher-order vibrations modes in electro-acoustical transducers. *Doctoral Thesis - Technische Universitat Dresden*, 2019.

[17] Nicolas Quaegebeur and Antonie Chaigne. Influence of material and shape on sound reproduction by an electrodynamic loudspeaker. *AES - 118th convention*, 2005.

[18] Sebastian Merchel Benjamin Zenker, Robert Schurmann and M. Ercan Altinsoy. Low-frequency performance of a woofer-driven flat-panel loudspeaker (part 1: Numerical system analysis and small signal measurement). *AES - 149th convention*, 2020.

[19] Zhi-Liang Zhang. Vibrations of loudspeaker cones in the transitional range. *Audio Engineering Society - Vol.54 No.7/8*, pages 589–603, 2006.

[20] Wolfgang Klippel. Diagnosis and remedy of nonlinearities in electrodynamical transducers. *AES - 109th convention*, 2000.

[21] Neville H. Fletcher and Thomas D. Rossing. *The Physics Of Musical Instruments*. Springer, 1998.

[22] Steve Errede. Vibrations of ideal circular membranes (e.g. drums) and circular plates. *406th Acoustical Physics of Music - UIUC Physics*, 2017.

[23] F. J. M. Frankort. Vibration and sound radiation of loudspeaker cones. *Doctoral Thesis*, 1975.

[24] F. J. M. Frankort. Vibration patterns and radiation behavior of loudspeaker cones. *Audio Engineering Society - Vol.26 No.9*, pages 609–622, 1978.

[25] Joachim Schlechter. Visualization of vibrations of loudspeaker membranes. *Degree Dissertation*, 2006.

[26] Murlan S. Corrington and Marshall C. Kidd. Amplitude and phase measurements on loudspeaker cones. *IRE Professional Group on Audio*, 1951.

[27] Wolfgang Klippel. Cone vibration poster. *www.klippel.de*, 2020.

[28] William A. Cardenas and Wolfgang Klippel. Loudspeaker rocking modes (part 1: Modeling). *www.klippel.de*, 2018.

[29] Wolfgang Klippel. Sound radiation poster. *www.klippel.de*, 2020.

[30] Wolfgang Klippel anf Joachim Schlechter. Measurement and visualization of loudspeaker cone vibration. *AES - 121th convention*, 2006.

[31] Joachim Schlechter Wolfgang Klippel. Distributed mechanical parameters of loudspeakers part 1: Measurements. *www.klippel.de*, 2009.

[32] Wolfgang Klippel and Joachim Schlechter. Distributed mechanical parameters of loudspeakers part 2: Diagnostics. *www.klippel.de*, 2009.

[33] Cobianchi Wolfgang Klippel Schwock, Cardenas. Root cause analysis of rocking modes in nonlinear domain. *AES - 142nd convention*, 2017.

[34] Ryan J. Mihelich. The effects of voice-coil axial rest position on amplitude modulation distortion in loudspeakers. *AES - 113th convention*, 2002.

[35] Wolfgang Klippel Mark Dodd and Oclee-Brown. Voice coil impedance as a function of frequency and displacement. *AES - 117th convention*, 2004.

[36] Wolfgang Klippel. Dynamical measurement of loudspeaker suspension parts. *www.klippel.de*, 2017.

[37] Wolfgang Klippel. Mechanical fatigue and load-induced aging of loudspeaker suspension. *www.klippel.de*, 2016.

[38] Finn Agerkvist and Bo R. Pedersen. Time varying behaviour of the loudspeaker suspension: Displacement level dependency. *AES - 127th convention*, 2009.

[39] Ulrik Skov and René Christensen. An investigation of loudspeaker simulation efficiency and accuracy using a conventional model, a near-to-far-field transformation and the rayleigh integral. *AES - 136th convention*, 2014.

[40] Huixian Cao and Zhiwen Chen. A novel and high efficient simulation model of loudspeaker. *AES - 148th convention*, 2020.

[41] Wolfgang Klippel. Hardware and software module of the klippel scanner analyzer system. *www.klippel.de*, 2022.

[42] Wolfgang Klippel. Scanning vibrometer (scn) manual. *www.klippel.de*, 2018.

[43] Wolfgang Klippel. Hardware and software module of the klippel scanner analyzer system - near field add-on. *www.klippel.de*, 2021.

[44] Polytec. Rc+ 7.0 user's guide. *www.polytec.com*, Sounds Good - Vibration Analysis is a Valuable Tool for Loudspeaker Development.

[45] Angelo Farina. Simultaneous measurement of impulse response and distortion with a swept-sine technique. *AES - 108th convention*, 2000.

[46] Jayant Datta Mark A. Martin and Xinhui Zhou. The evolution of chirp-based measurement techniques. *AES - 144th convention*, 2018.

[47] Angelo Farina. Advancements in impulse response measurements by sine sweeps. *AES - 122nd convention*, 2007.

[48] Angelo Farina Daniel Pinardi Maria Costanza Bellini, Luca Collini and Kseniia Riabova. Measurements of loudspeakers with a laser doppler vibrometer and the exponential sine sweep excitation technique. *Audio Engineering Society*, pages 600–612, 2017.

[49] Pierrick Lotton Antonin Novak and Laurent Simon. Synchronized swept-sine: Theory, application and implementation. *Audio Engineering Society - Vol.63 No.10*, pages 786–798, 2015.

[50] Wolfgang Klippel and Joachim Schlechter. Dynamical measurement of the effective radiation area sd. *www.klippel.de*, 2016.

[51] Angelo Farina Alessio Figuretti Anna Tira, Daniel Pinardi and Davide Palmieri. Experimental and numerical methods for the evaluation of sound radiated by vibrating panels excited by electromagnetic shakers in automotive applications. *MDPI*, 2022.

[52] René Christensen. Phase decomposition for loudspeaker analysis. *COMSOL Multiphysics Conference*, 2016.

[53] EPSON. T series robot manual. *www.epson.com*, 2022.

[54] EPSON. Rc+ 7.0 user's guide. *www.epson.com*, 2022.

[55] EPSON. Spel+ language reference. *www.epson.com*, 2022.

List of Figures

Ringraziamenti

Dopo aver conseguito anche questo titolo, finalmente oggi, dopo 36 esami, 2 tesi, un Corso di Perfezionamento ed uno stage in azienda, si conclude definitivamente il mio percorso universitario.

In questi anni ho superato esami interessanti e formativi ed esami inutili e logoranti.
Ho avuto docenti volenterosi e preparati e "baroni" incompetenti ed arroganti. Ho imparato a relazionarmi con diversi tipi di persone, a prendere talvolta ispirazione da esse ed a gestire situazioni stressanti al fine di raggiungere gli obiettivi prefissati.

Ho acquisito conoscenze che spero di poter utilizzare nella mia professione ed ho fatto affidamento ad esperienze personali e corsi extra-accademici per acquisire quelle competenze necessarie al completamento di una figura professionale che l'università non è stata in grado di fornirmi.

Ora che finalmente è tutto finito, posso cominciare a guardare al mio futuro ed iniziare davvero a vivere la mia vita. Spero di poter presto avere la possibilità riprendere le passioni e le attività che ho dovuto mettere da parte per fare spazio allo studio. Mi auguro che tutti gli sforzi compiuti, le rinunce fatte ed i fine settimana passati rinchiuso in una stanza a studiare possano con il tempo trovare una giusta ricompensa e garantirmi un futuro tranquillo, felice ed economicamente appagante.

L'unica cosa di cui ora sono certo e di cui posso ritenermi soddisfatto è che ho sempre seguito le mie passioni e fatto le migliori scelte che potessi fare sulla base di esse.

Desidero estendere il mio sincero apprezzamento a Eighteen Sound e B&C Speakers per avermi gentilmente permesso di svolgere questa tesi magistrale presso le loro aziende. Il loro sostegno e la loro collaborazione sono stati fondamentali per il successo di questo lavoro. Sono grato per i preziosi consigli e l'assistenza fornita nonché per la dedizione e l'entusiasmo con cui sono stato seguito in questi mesi. Ringrazio in maniera particolare Marco, Filippo e Fabio per il loro supporto e per le preziose nozioni che sono riusciti a trasmettermi.

Ringrazio mia madre e mio padre per il supporto morale ed economico. Ringrazio in particolar modo Alessandra (visto che nella tesi triennale non l'avevo esplicitamente ringraziata e ci era rimasta male) per il sostegno e per i video degli animali condivisi da TikTok.

Ringrazio tutti i miei nonni. Sebbene non siano qui presenti, la loro vicinanza spirituale mi ha sostenuto ed ha contribuito a farmi arrivare fin qui.

Ringrazio i miei zii e i miei cugini che sono stati presenti quando avevo bisogno di un consiglio o di svagarmi.

Ringrazio i miei colleghi del Politecnico. Senza il lavoro di squadra che abbiamo fatto adesso non sarei qui. In particolare ringrazio Alessio, Mattia, Miriam, David, Federico, Wendy, Enrico, Hakim, Jacopo e Gerardo. Passo dopo passo ho costruito tutto questo anche grazie a voi.

Ringrazio tutte le persone, gli amici ed i conoscenti che mi sono vicini e quelli che sono passati temporaneamente nella mia vita per poi allontanarsi. Ognuno di voi ha lasciato un segno in me e sono grato per tutte le esperienze condivise. Siete stati parte integrante del mio percorso ed avete contribuito a farmi crescere e diventare la persona che sono oggi.

Infine, ringrazio me stesso. Senza la passione e la testardaggine che mi contraddistinguono non sarei mai arrivato a questo punto. Questo percorso mi ha dato la possibilità di mettermi in gioco e mi ha mostrato come potessi ottenere risultati che non avrei mai creduto di poter raggiungere.